Construction and Building Materials 537 (2026) 147166

Contents lists available at ScienceDirect

Construction and Building Materials

journal homepage: www.elsevier.com/locate/conbuildmat

Form-stable PCMs in lime renders: From particle-matrix interactions to thermal buffering and durability

Andrea Rubio-Aguinaga, Loucas Kyriakou, José María Fernández, Íñigo Navarro-Blasco, José Ignacio Álvarez *

MATCH Research Group, Department of Chemistry, School of Sciences, University of Navarra, C/. Irunlarrea 1, Pamplona 31008, Spain

ARTICLE INFO

Keywords:
Form-stable phase change materials (PCMs)
Silica-supported PCMs
Lime renders
Microstructural interactions
Energy efficiency
Thermal buffering
Durability

ABSTRACT

The development of thermally responsive lime renders has been constrained by the lack of materials capable of storing and releasing heat without compromising compatibility, durability or the microstructural integrity required in both modern and heritage applications. Although form-stable phase change materials (PCMs) offer a promising route for latent-heat storage, their behaviour within lime matrices remains insufficiently explored. This study addresses this gap through a comprehensive, multi-scale investigation of lime renders incorporating silica-supported PCMs, linking particle-level interactions to thermal performance and long-term durability. Two PCMs with distinct melting temperatures (5°C and 25°C) were integrated into optimised lime formulations. The results reveal that the silica carriers exhibit excellent compatibility with the lime system, enabling uniform PCM dispersion and preserving a continuous and stable microstructure. Contrary to concerns commonly associated with PCM integration, the modified mortars improved their mechanical performance and displayed no disruption to the pore network essential for durability in lime-based materials. Both PCMs remained fully functional within the hardened matrix, providing reversible latent-heat storage and measurable temperature buffering under dynamic conditions. Enhanced thermal moderation was achieved without compromising durability: PCM-modified mortars outperformed control samples under freeze-thaw cycling and salt crystallisation, with the strongest improvements observed in formulations containing metakaolin. The PCMs themselves demonstrated excellent cycling stability, preserving their thermal response over repeated phase transitions. These findings demonstrate that silica-supported PCMs can be effectively integrated into lime renders to deliver meaningful thermal regulation while maintaining compatibility, structural integrity, and long-term performance, highlighting their potential for energy-responsive and heritage-compatible construction materials.

1. Introduction

The building sector is responsible for a substantial share of global energy consumption and greenhouse gas emissions, largely due to the heating and cooling demands in indoor environments [1]. In Europe, buildings account for approximately 40% of total energy demand and 36% of CO_2 emissions, prompting an urgent shift toward energy-efficient and sustainable construction practices [1,2]. Policy frameworks such as the European Green Deal and the recast Energy Performance of Buildings Directive (EPBD) call for the decarbonisation of the built environment, highlighting the renovation and retrofitting of existing buildings as essential pathways toward carbon neutrality by 2050 [3–5]. Improving the thermal performance of building envelopes is therefore a priority for reducing operational energy needs and mitigating environmental impacts [6–9]. However, most conventional construction materials exhibit limited thermal inertia and cannot actively moderate temperature fluctuations across daily and seasonal cycles. This limitation underscores the need for new materials capable of passively storing and releasing heat, thereby contributing to stabilised indoor temperatures and reduced energy demand peaks [10–12].

Phase change materials (PCMs) have emerged as a promising passive strategy for enhancing building thermal performance [13–18]. By absorbing and releasing latent heat during phase transitions, PCMs can buffer indoor temperature variations and decrease the frequency and intensity of heating and cooling peaks [13–18]. Their incorporation into construction materials, such as concrete, gypsum, cement, and mortars, has been extensively investigated, with many studies demonstrating improvements in thermal comfort and energy loads [13–18].

* Correspondence to: Departamento de Química, Facultad de Ciencias, Universidad de Navarra, C/ Irunlarrea, 1, Pamplona, Navarra 31008, Spain.
E-mail address: jalvarez@unav.es (J.I. Álvarez).

https://doi.org/10.1016/j.conbuildmat.2026.147166
Received 17 December 2025; Received in revised form 30 April 2026; Accepted 18 June 2026
Available online 23 June 2026

Nevertheless, practical implementation remains challenging. The effectiveness of PCM-enhanced materials depends not only on the thermal characteristics of the PCM but also on the incorporation method, compatibility with the host matrix, and long-term stability of the composite [19,20].

Several strategies exist for integrating PCMs into building materials [15,20–24]. In macroencapsulation, PCMs are contained in large enclosures or tubes embedded within walls or panels. While this prevents direct contact with the binder, it introduces thermal resistance and limits design flexibility [23]. Microencapsulation surrounds PCM droplets with polymeric shells on the micrometre scale, enabling uniform dispersion and preventing leakage [24]. However, these shells are vulnerable to mechanical damage during handling or mixing, potentially leading to PCM leakage and deterioration of physical and mechanical properties of the composite [23,24]. A third approach, known as form-stable or shape-stabilised PCMs, relies on physically confining molten PCM within a porous solid support that acts as a structural framework [25–29]. These supporting matrices can be inorganic (silica, diatomite, perlite, expanded graphite) or organic/polymeric (polyethylene, polyurethane, polymethyl methacrylate (PMMA), etc.) [25–29]. In this system, the PCM remains immobilised within the pore network even above its melting point, preventing leakage without the need for encapsulating shells. Form-stable PCMs allow higher PCM loadings, improved thermal conductivity (depending on the support), simplified manufacturing, and enhanced structural stability [30–32]. Despite these advantages, studies on form-stable PCM incorporation remain limited, particularly in lime-based systems.

Lime mortars have regained attention for their environmental benefits and compatibility with both modern and historical masonry [33,34]. Air lime has substantially lower embodied energy and CO_2 emissions than Portland cement and partially reabsorbs CO_2 during carbonation, acting as a carbon sink [34–37]. Lime mortars also exhibit high vapour permeability, self-healing capability, and compatibility with traditional substrates such as brick, limestone, and sandstone [19,33] making them ideal for conservation and restoration works, where mechanical and chemical compatibility are essential [33]. However, their inherently poor thermal performance and their limited capacity to moderate temperature variations, limits their contribution to energy efficient building design. Integrating PCMs into lime mortars could therefore deliver dual environmental benefits by combining lime's low-carbon characteristics with the thermal energy storage capacity of PCMs [13,14,24,38].

Over the past decade, research on PCM-integrated building materials has predominantly focused on microencapsulated systems, which are readily available in well-defined particle sizes and melting ranges and easy to incorporate [16,17,24,39–45]. Their addition to cementitious and gypsum matrices has been shown to improve indoor thermal stability and reduce energy loads [17,39–41,43–45]. Fewer studies, however, have examined their behaviour in lime-based systems [16,24,42]. While recent work confirms that microencapsulated PCMs can enhance the temperature-buffering capacity of lime mortars with minimal mechanical degradation [16,24,42], their low incorporation limits and susceptibility to capsule rupture can restrict their practical effectiveness.

Form-stable PCMs supported on porous inorganic or polymeric matrices have attracted increasing interest in cement-based composites [46–49], yet their application in lime systems remains scarcely explored [25,50]. Their integration presents both opportunities and challenges. Silica-supported PCMs can enable higher PCM loadings, greater dimensional stability, and potentially superior thermal performance compared with microencapsulated systems. However, their interactions with the lime matrix, and their effects on microstructure, strength development, and thermal behaviour, remain largely unexplored. Determining whether the benefits observed in cement-based composites translate to lime mortars is essential for advancing their use in heritage restoration and energy-efficient construction.

Most existing studies also focus primarily on the thermal aspects of PCM incorporation, often without linking thermal behaviour to compatibility and interaction phenomena, microstructural evolution, mechanical performance, or durability under cyclic exposure. This fragmented approach limits the predictive capacity and practical applicability of the findings. A comprehensive, multi-scale methodology is therefore needed, one that correlates compatibility and interactions with microstructure, mechanical properties, thermal buffering efficiency, and long-term durability. Such an approach is particularly critical for sustainable restoration, where materials must simultaneously satisfy energy efficiency, environmental, and heritage compatibility criteria [13,51]. Such knowledge is essential not only for advancing material design but also for guiding the formulation of thermally enhanced lime renders for conservation and low-carbon retrofitting.

This research addresses these gaps through a rigorous, integrated investigation of lime mortars incorporating silica-supported form-stable PCMs. Two paraffin-based PCMs with melting points of 5 °C and 25 °C were supported on porous silica and added to lime mortars at controlled dosages. This study examines the full performance chain, from particle-level interactions, dispersion, and zeta potential to microstructural development, mechanical behaviour up to one curing year, and thermal performance assessed through thermal conductivity, differential scanning calorimetry, and dynamic hotbox experiments. Durability and thermal cycling stability are further evaluated to determine long-term functionality. By integrating these dimensions, the work provides a holistic understanding of how silica-supported PCMs behave within lime matrices and establishes guidelines for developing high-performance, low-carbon, and heritage-compatible mortars for energy-efficient building envelopes.

2. Materials and methods

2.1. Materials

Air lime mortars were prepared using hydrated calcitic lime (CL90-S, Cal Industrial S.A., Navarra, Spain) as the binder and a calcareous sand (CTH Navarra, Spain) with a particle size range of 0–1 mm as the fine aggregate. The hydrated lime exhibited a mean particle size of approximately 10 μm, with fewer than 10% of particles exceeding 50 μm. The sand presented a well-graded, high-purity calcareous composition. A constant binder-to-aggregate ratio of 21.7/78.3 by weight was used for all formulations, and the mixing water was fixed at 25 wt% to enable meaningful comparison across mixtures.

Chemical and mineralogical characterisation of raw materials was carried out by X-ray fluorescence (XRF) and X-ray diffraction (XRD). XRF analyses were performed using a Bruker S2 Puma spectrometer equipped with a silver-anode X-ray tube and a 4 μm polypropylene filter under a helium atmosphere, with quantification via Spectra Results Manager software. The hydrated lime contained 96.5% CaO, 1.3% SO_3, 0.9% MgO and 0.8% SiO_2, with portlandite ($Ca(OH)_2$) as the dominant crystalline phase and calcite ($CaCO_3$) as secondary. The calcareous sand consisted mainly of calcite ($CaCO_3$), with minor quartz (SiO_2), montmorillonite and hydrobiotite phases, and an oxide composition of 94.6% CaO, 2.3% SiO_2, 0.8% Al_2O_3 and 0.7% MgO.

To optimize the fresh and hardened properties of the mortars, three additives were incorporated: a carboxylate ether-based superplasticiser (MasterCast GT 205, Master Builders Solutions, Spain) to enhance fluidity and reduce water demand; a starch-derived adhesion promoter (Casaplast KO09 S, Nova Casanova, Spain) to improve cohesion and adhesion to the substrate; and metakaolin (Metaver N, NEWCHEM, Austria), added at 20% by weight of lime (bwol) in selected mixes, as a pozzolanic admixture. XRF analysis of the metakaolin (MK) revealed an oxide composition of 49.3% Al_2O_3, 45.4% SiO_2, 1.9% MgO, 0.9% K_2O, 0.9% Fe_2O_3 and 0.8% Na_2O.

To enhance thermal regulation, two silica-supported form-stable phase change materials (PCMs) were incorporated at a fixed dosage of 10% bwol. Both materials (Rubitherm GmbH, Germany) consist of

paraffinic compounds physically retained within a porous silica matrix, preventing leakage during phase transition. According to the manufacturer, the silica carrier has an average particle size of approximately 200 μm. The PCMs, designated PCM5 and PCM25, exhibit melting temperatures of 5 °C and 25 °C, respectively, allowing the evaluation of silica-supported form-stable PCM-lime mortars across a broader range of thermal activation conditions and providing comparative insight into the influence of transition temperature on material performance. This approach not only enables assessment of PCM systems within more conventional building-related transition ranges, but also expands understanding of lower-transition-temperature materials, thereby broadening the scientific basis for future optimization of single- and multi-PCM formulations designed for diverse climatic and operational scenarios.

2.2. Mortar preparation

To ensure homogeneous dispersion, the dry constituents, including lime, sand, metakaolin (MK) when applicable, the adhesion promoter, the PCMs, and an initial 0.25% bwol of superplasticiser, were blended for 5 min in a Lleal BL−8-CA solid-additives mixer (Granollers, Spain). The predetermined water content of 25 wt% was then added using a Proeti ETI 26.0072 planetary mixer (Madrid, Spain) operating at low speed for 270 s. During mixing, additional increments of superplasticiser were introduced until the mortar achieved the consistency required for rendering applications, as evaluated by the flow-table test [52].

Once the desired workability was achieved, the fresh mortar was applied as a 0.5 cm-thick render onto saturated calcareous bricks (DICONA, Pamplona, Spain). The renders were then covered with a plastic film for 15 days to prevent excessive moisture loss. After the curing period, the film was removed and the adhesion, shrinkage and cracking behaviour were examined. These characteristics were classified according to a qualitative scale previously established by the authors [16,19], ranging from Degree 3 (excellent adhesion and no visible cracks) to Degree 0 (poor adhesion with deep and extensive cracking). The observations were used to adjust the superplasticiser and additive contents until an optimised formulation with improved spreadability, cohesion and adhesion was obtained.

Following optimisation, the mortars were cast into specimens and cured under controlled laboratory conditions (20 ± 0.5 °C and 60 ± 5% RH). Specimens were prepared in three geometries corresponding to the different tests: discs (Ø = 55 mm; thickness = 20 mm) for thermal conductivity measurements; cylinders (Ø = 30 mm; h = 40 mm) for mechanical, microstructural and durability analyses; and rectangular slabs (9 × 18 cm; 2 cm thick) for hot-box thermal-efficiency experiments.

After curing, the specimens were freeze-dried to halt carbonation and hydration reactions at specific curing ages. The procedure consisted of immersion in liquid nitrogen for 5 min, followed by sublimation at −40 °C under 1 Pa vacuum for 24 h, ensuring preservation of the mortars' microstructural features.

2.3. Compatibilities and interactions evaluation

2.3.1. Particle size distribution

The particle size distribution of the materials was characterised by laser diffraction using a Malvern Mastersizer (Malvern Panalytical Ltd., Malvern, UK). The analysis aimed to evaluate dispersion behaviour and potential interactions among the particles. Three experimental groups were examined:

- The first group assessed interactions between the PCMs and the chemical additives. Aqueous dispersions containing 10 wt% PCM were prepared with increasing amounts of superplasticiser (0, 0.50, 0.75, 1.00 and 1.50%, by weight of PCM) or starch-based adhesion promoter (0, 0.25, 0.50 and 0.75%, by weight of PCM). An equivalent series of suspensions was prepared for systems containing metakaolin, maintaining a metakaolin-to-PCM mass ratio of 2:1, reflecting the proportions used in the mortar formulations.
- The second group examined interactions between the PCMs and the lime matrix in the presence of the additives. Suspensions containing 5 wt% lime and 10% bwol PCM were prepared and combined with the same range of superplasticiser or starch derivative dosages. The procedure was repeated for systems containing 20% bwol metakaolin to determine the influence of MK on particle interactions.
- The third set of experiments evaluated the combined effect of the superplasticiser and the adhesion promoter in the presence of lime and PCMs. Aqueous suspensions containing 5 wt% lime, 10% bwol PCM, and a fixed 0.50% bwol of the adhesion promoter were prepared, while the amount of superplasticiser was varied (0, 0.75 and 1.50% bwol). These experiments were also conducted on mixtures containing 20% bwol metakaolin to simulate the interactions occurring in the complete mortar matrix.

2.3.2. Optical microscopy

To complement the laser particle size analysis, the interactions among chemical additives, PCMs and the lime matrix were further examined by optical microscopy using a Zeiss Axiolab 5 optical microscope (Carl Zeiss Microscopy, Oberkochen, Germany). This technique enabled visual inspection of the particle morphology, agglomeration phenomena, and the degree of PCM dispersion within the suspensions. All samples were analysed in duplicate, and the images presented correspond to representative observations consistently identified across both replicates.

2.3.3. Zeta potential

The electrostatic behaviour of the suspensions was assessed through zeta potential measurements using a ZetaProbe analyser (Colloidal Dynamics, Ponte Vedra Beach, FL, USA), which operates based on the electro-acoustic technique. Zeta potential was used to characterise the balance between attractive and repulsive forces governing particle interactions, providing insight into the colloidal stability and compatibility of the PCM-lime systems.

The measurements were conducted on aqueous suspensions representative of the optimised mortar formulations, allowing the evaluation of the combined electrostatic interactions between the binder, PCMs and chemical additives. Suspensions containing 5 wt% lime, 10% bwol PCM (PCM5 or PCM25), and 0.75% bwol superplasticizer were prepared and titrated with 1 wt% starch-based adhesion promoter. The same procedure was repeated for mixtures incorporating 5 wt% lime and 20% bwol metakaolin. This approach enabled the characterisation of the electrostatic behaviour of the fully combined PCM–lime systems under conditions directly relevant to the optimised mortar compositions.

2.4. Fresh state tests

The behaviour of the mortars in the fresh state was evaluated through a series of standardised tests. Flowability was assessed using the flow-table method in accordance with UNE-EN 1015–3 [52], while density and entrapped air content were measured following UNE-EN 1015–6 [53] and UNE-EN 1015–7 [54], respectively. Water retention capacity was determined according to the Spanish standard UNE 83–816–93 [55]. Collectively, these measurements provided a comprehensive assessment of the fresh-state properties of the mortars and enabled direct comparison among the different formulations.

2.5. Microstructure characterization

2.5.1. Specific surface area (BET)

The textural properties of the form-stable PCMs (PCM5 and PCM25) were characterised by nitrogen adsorption-desorption at 77 K using an ASAP 2020 analyser (Micromeritics GmbH, Mönchengladbach, Germany). Prior to measurements, samples were degassed under vacuum at

95 °C for 24 h. Both PCM types were analysed to evaluate their surface characteristics and to identify possible differences associated with their morphology and particle structure. Approximately 0.1 g of each pure powdered PCM was used for analysis, which was considered fully representative of the bulk material due to the intrinsic homogeneity of the supplied samples. The specific surface area was obtained using the multipoint Brunauer-Emmett-Teller (BET) method, while the mesopore size distribution and cumulative pore volume were derived from the adsorption branch using the Barrett-Joyner-Halenda (BJH) method.

2.5.2. Mercury intrusion porosimetry (MIP)

The pore structure of the mortars was analysed by mercury intrusion porosimetry (MIP) to assess the influence of PCM incorporation on microstructural features. Measurements were performed using a Micromeritics AutoPore IV 9500 porosimeter (Micromeritics Instrument Corp., Norcross, GA, USA) within a pressure range of 0.0015–207 MPa. For each test, small cubic fragments of approximately 1 cm per side were selected to ensure consistent geometry and reliable penetration of mercury throughout the pore network. All analyses were performed in duplicate for each composition to ensure reproducibility and representative microstructural characterization.

2.5.3. Scanning electron microscopy (SEM)

Microstructural observations were performed using a COXEM EM-30N scanning electron microscope (COXEM Co. Ltd., Daejeon, South Korea), equipped with secondary electron (SE) and backscattered electron (BSE) detectors to visualise surface morphology and compositional contrast. Elemental analysis was conducted with an energy-dispersive X-ray spectroscopy (EDS) detector (Quantax Compact30, Bruker Corporation, Billerica, MA, USA), and spectra were processed using Esprit Compact software. Prior to examination, samples were coated with a thin gold layer using a COXEM SPT−20 ion sputter coater to enhance electrical conductivity and image resolution. All samples were examined in duplicate, and the micrographs presented correspond to representative observations consistently identified across the analysed replicates.

2.6. Mechanical performance: compressive strength

The compressive strength of the mortars was determined using a Frank/Controls 81565 testing press fitted with a Proeti ETI 26.0052 compressive breaking device. Tests were performed at loading rates between 10 and 50 N/s, with a total loading duration of 30–90 s to ensure consistent testing conditions. Mechanical performance was evaluated after 28, 91, 182 and 365 days of curing to monitor strength development over time. For each condition, three cylindrical specimens were tested, and the average value and standard deviation were calculated to assess reproducibility and experimental reliability.

2.7. Thermal performance assessment

2.7.1. Thermal conductivity

Thermal conductivity (λ) was determined using a FOX50 Heat Flow Meter (TA Instruments), equipped with two independently controlled Peltier plates that maintain a constant temperature gradient of 10 °C across the sample. Discs (Ø = 55 mm; thickness = 20 mm) cured for at least 28 days were tested to ensure microstructural stability. Measurements were taken at −5°C, 5 °C, 15 °C, 25 °C and 35 °C to capture the thermal response of the mortars across temperature ranges corresponding to the solid and liquid states of the PCMs. For each formulation, three specimens were analysed, and the mean value and standard deviation were reported to ensure measurement consistency.

2.7.2. Differential scanning calorimetry (DSC)

The phase-change behaviour of the PCMs was analysed by differential scanning calorimetry (DSC) to determine the melting (ΔH_m) and crystallization (ΔH_c) enthalpies, together with the corresponding melting (T_m) and crystallization (T_c) temperatures. Additionally, the onset and endset temperatures of both melting and crystallization processes were evaluated to more comprehensively define the full operational temperature ranges of latent heat storage and release. Measurements were performed using a DSC25 calorimeter (TA Instruments), and data were processed with TRIOS software. Each sample underwent three consecutive heating-cooling cycles between −20 °C and 50 °C at a rate of 5 °C/min. To eliminate the effect of thermal history and ensure temperature stabilisation, a 5-minute isothermal step was included at both the beginning and the end of each cycle [56–58]. Approximately 15 mg of sample was placed in standard aluminium pans with lids. This sample quantity was considered fully representative due to the homogeneous powdered nature of the pure PCM materials. Measurements were conducted under nitrogen flow at 50 mL/min, with an additional purge of approximately 400 mL/min, ensuring thermal stability and reliable heat-flow readings.

2.7.3. PCM leakage test

One relevant aspect of the thermal behaviour of form-stable PCMs is their ability to retain the paraffinic phase within the porous matrix when exposed to temperatures above the melting point, as the PCM is fully in the molten state. Following leakage evaluation methodologies commonly reported in previous form-stable PCM studies [59,60], the potential leakage of PCM5 and PCM25 was evaluated by placing 1 g of each material on pre-weighed filter substrates and maintaining them at 40 °C and 75 °C for 1 h, conditions selected to ensure complete melting of the paraffinic phase. The selected sample mass was considered fully representative due to the intrinsic compositional homogeneity of the pure PCM powders. After cooling to room temperature, the substrates were visually inspected for halos or wetting marks indicative of paraffin release and subsequently reweighed to quantify any mass variation associated with PCM migration. This combined qualitative and quantitative assessment enabled the evaluation of possible leakage when the PCM is in its liquid state.

2.7.4. Energy efficiency

The thermal efficiency of the PCM-containing mortars was assessed using a hotbox experimental setup designed to simulate realistic thermal conditions, following methodologies previously validated in the literature [16,24,41,61,62]. Four flat mortar slabs (9 × 18 cm; 2 cm thick) were mounted inside a thermally insulated expanded polystyrene box (Fig. 1), which was sealed with high-temperature resistant silicone to ensure controlled heat transfer through the mortar surfaces, in line with established procedures [16,24]. This configuration allowed heat transfer across multiple interfaces, effectively reproducing the multidirectional heat exchange characteristic of building envelope systems.

Two hotboxes were placed inside a climatic chamber and subjected to cyclic temperature variations between −10 °C and 50 °C to replicate extreme outdoor-like conditions (Fig. 1). One hotbox contained the PCM-enhanced mortar, while the other, prepared with PCM-free mortar, served as the control. Thermocouples positioned within each box and inside the climatic chamber continuously recorded temperature evolution, enabling a direct comparison of the thermal regulation performance of the two systems.

The recorded data were processed using OriginLab software, and temperature differentials (ΔT) between the PCM and control hotboxes were calculated as a function of time. To quantify the relative thermal response, the area under the ΔT-time curve was determined by numerical integration, as expressed in Eq. (1). The resulting parameter, expressed in °C·s, provides a comparative indicator of the PCM's capacity to moderate temperature fluctuations throughout the test period.

$$Q^* = \int_{t1}^{t2} \Delta T(t)dt \quad (1)$$

This approach enabled a comprehensive evaluation of the thermal

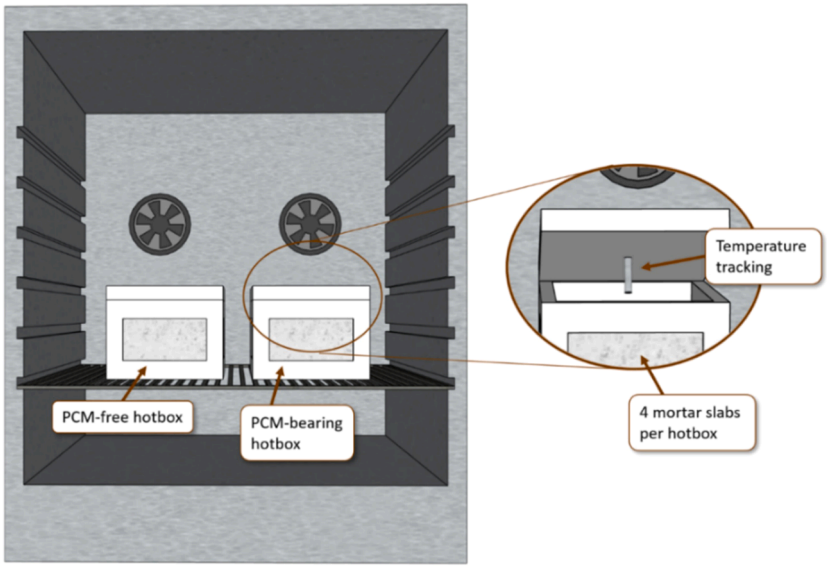

Fig. 1. Hotbox experimental assembly inside the climatic chamber.

buffering effect of PCM-enhanced mortars under dynamic conditions, allowing estimation of their relative ability to reduce temperature peaks and improve energy efficiency.

2.8. Durability and cyclability

2.8.1. Durability assessment

The long-term durability of the mortars was evaluated through accelerated ageing procedures following two complementary methods: freeze-thaw cycling and salt crystallization.

For the freeze-thaw resistance test, specimens were subjected to repeated cycles consisting of immersion in water at room temperature for 24 h, followed by freezing at −20 °C for an additional 24 h in a Samsung RZ80FJSW freezer, following an adapted procedure based on EN 1367–1 [63]. This two-step cycle was repeated for up to 28 cycles or until complete failure of the specimens.

Salt crystallization resistance was assessed by immersing the specimens in a saturated magnesium sulphate ($MgSO_4$) solution at 20 °C and 95% relative humidity for 24 h, followed by drying at 110 °C for an additional 24 h, following an adapted protocol based on EN 1367–2 [64]. To prevent excessive salt accumulation on the specimen surfaces, a rinsing step was carried out every 10 cycles. The test continued for a maximum of 28 cycles or until total disintegration of the samples.

Cylindrical specimens (Ø = 30 mm; h = 40 mm) were prepared in duplicate for each durability protocol. Visual inspections were performed after each cycle to document the progression of deterioration. Damage was classified according to a previously established qualitative scale (Table 1), allowing consistent comparison among the different mortar formulations [16,65]. In parallel, the mass of the specimens was measured after each cycle to quantitatively monitor the deterioration over time.

2.8.2. Thermal cycling stability

To complement the durability assessment, thermal cycling tests were carried out to evaluate the long-term stability of the PCMs under repeated thermal stress. The analysis was performed by DSC using the same experimental configuration described in Section 2.7.2, with the exception of the heating/cooling rate and the number of cycles. The PCMs were subjected to 40 consecutive heating and cooling cycles between −10 °C and 50 °C at a rate of 20 °C/min. This elevated scanning rate was selected to establish an accelerated cyclability protocol within a reasonable experimental timeframe, enabling rigorous assessment of thermal resilience under repeated phase transition conditions. Under this framework, the principal objective was the evaluation of potential

Table 1
Damage scale and visual assessment of durability tests.

Damage scale (0-10)	Characteristics
0	No visible damage; specimen intact.
1	Minimal material loss; almost no damage.
2	Small cracks; slight material loss.
3	Moderate cracks; visible wear.
4	Larger cracks; significant material loss.
5	Major cracks; pronounced material loss.
6	Severe cracks; surface starting to break apart.
7	Large sections missing; extensive cracking.
8	Structure heavily compromised; crumbling.
9	Near total destruction; disintegration visible.
10	Total destruction; specimen turned to dust.

progressive degradation, thermal fatigue, or latent heat loss throughout successive cycles, rather than detailed characterisation of intrinsic phase transition behaviour. The evolution of the melting (ΔH_m) and crystallization (ΔH_c) enthalpies was monitored throughout the cycling process to identify potential degradation or reductions in latent heat storage and release capacity. Standard deviations were calculated to assess the consistency of the thermal response and provide a quantitative indicator of stability across the 40 cycles.

3. Results and discussion

3.1. Interactions and compatibility among additives

Understanding the interactions among all components of the system is essential for predicting their collective behaviour and for designing optimised lime mortars incorporating phase change materials. However, the compatibility of silica-supported form-stable PCMs with key admixtures typically used in lime mortars remains unreported. To address this gap, their interactions with the superplasticiser, the starch-based adhesion promoter and metakaolin were evaluated using particle size analysis, optical microscopy and zeta potential measurements to determine their stability.

The intrinsic granulometric profiles of PCM5 and PCM25, detailed in Supplementary Material (Figure S1), were used as a reference to assess the influence of the admixtures. Both PCMs preserved their characteristic size distributions upon addition of the superplasticiser or the starch-based adhesion promoter, with no peak shifts or signs of alteration of the physical integrity or dispersion state, confirming their physical stability in the presence of these additives. In MK-bearing systems, the PCMs again remained unaffected, although the starch derivative induced a slight agglomeration of MK, visible as an additional intermediate peak.

In lime-PCM suspensions (Fig. 2), systems without additives exhibited distinct particle populations, arising from the simple coexistence of the two components. This observation confirms the absence of direct interactions between the lime particles and the PCMs. In PCM5 suspensions containing superplasticiser (Fig. 2a), increasing dosage produces a progressive shift of the lime-related distribution towards smaller particle sizes, together with a noticeable decrease in the intensity of the PCM-related peak. This behaviour is consistent with enhanced dispersion induced by the superplasticizer. In PCM25 systems (Fig. 2c), this effect is more subdued due to the inherently multimodal nature of PCM25, whose dominant modes partially overlap the granulometric range of lime, making size-related changes less discernible. In contrast, addition of starch-based adhesion promoter results in particle size distributions that progressively shift towards larger diameters (Fig. 2b for PCM5 and Fig. 2d for PCM25). This trend, consistent with previously reported behaviour for starch derivatives [19], reflects an overall increase in the apparent particle size of the suspensions.

In systems containing both lime and metakaolin (Fig. 3), the addition of superplasticiser again induced a shift towards smaller particle sizes for both PCM5 and PCM25 (Fig. 3a and Fig. 3c). In the PCM5 systems (Fig. 3a), a fine-size population emerged upon superplasticiser addition but remained essentially unchanged across all dosages, indicating that the overall suspension structure was only modestly affected. For PCM25 (Fig. 3c), a slight shift towards smaller sizes was also observed when compared with the additive-free system, although the effect was subtler. In contrast, the starch-based adhesion promoter caused the particle size distributions to shift progressively towards larger diameters for both PCM5 and PCM25 (Fig. 3b and Fig. 3d), mirroring the behaviour observed in lime-only suspensions and indicating an overall increase in apparent particle size in the presence of this additive.

Finally, multicomponent suspensions combining lime, PCM, superplasticiser and starch-based adhesion promoter, with and without metakaolin, were analysed to better represent the compositional complexity of real lime mortars (Supplementary Material, Figure S2). Across all formulations, the particle size distributions remained stable and showed a consistent shift towards smaller diameters with increasing superplasticiser dosage, reflecting effective dispersion under multicomponent conditions. The reproducibility of this behaviour for both PCM types and binder compositions confirms the granulometric stability of these complex systems.

The observations obtained from the particle size analysis were further supported by optical microscopy of the same suspensions (Fig. 4). In the presence of the superplasticiser, the micrographs reveal a

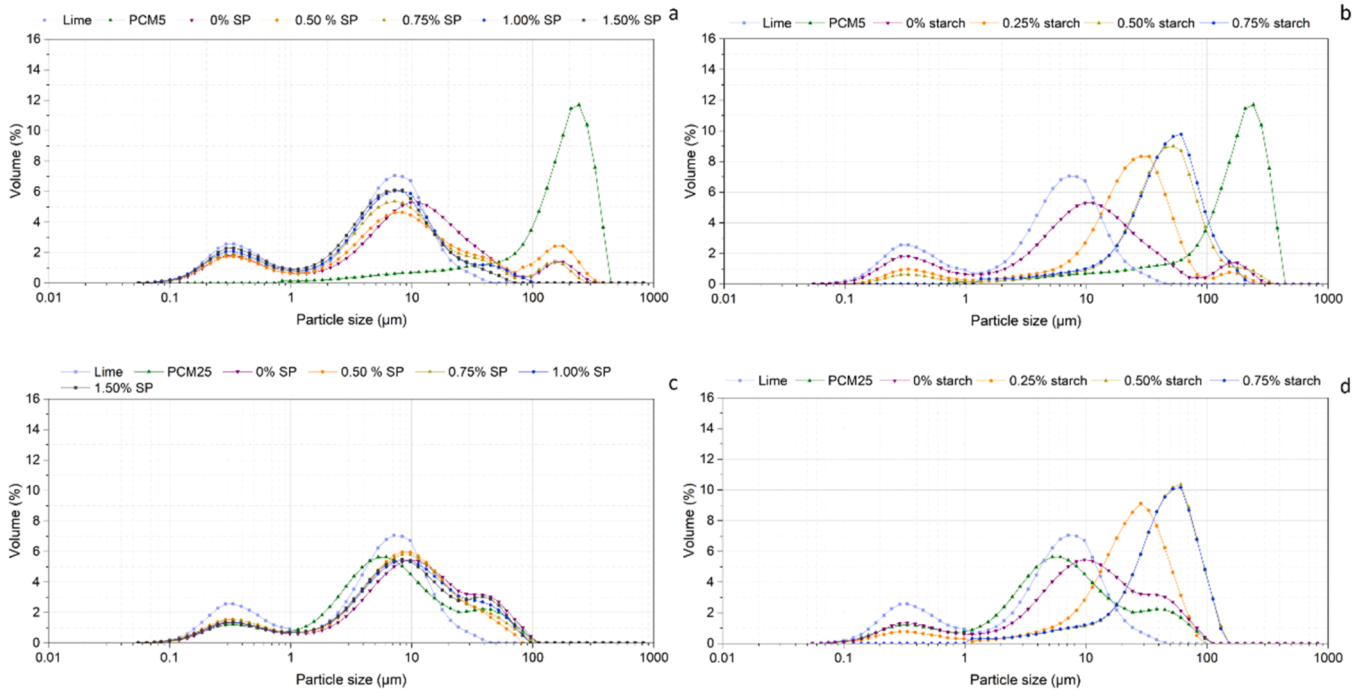

Fig. 2. Particle size distributions of aqueous lime suspensions containing: (a) PCM5 with increasing dosages of superplasticiser, (b) PCM5 with increasing dosages of starch based additive, (c) PCM25 with increasing dosages of superplasticiser, and (d) PCM25 with increasing dosages of starch based additive.

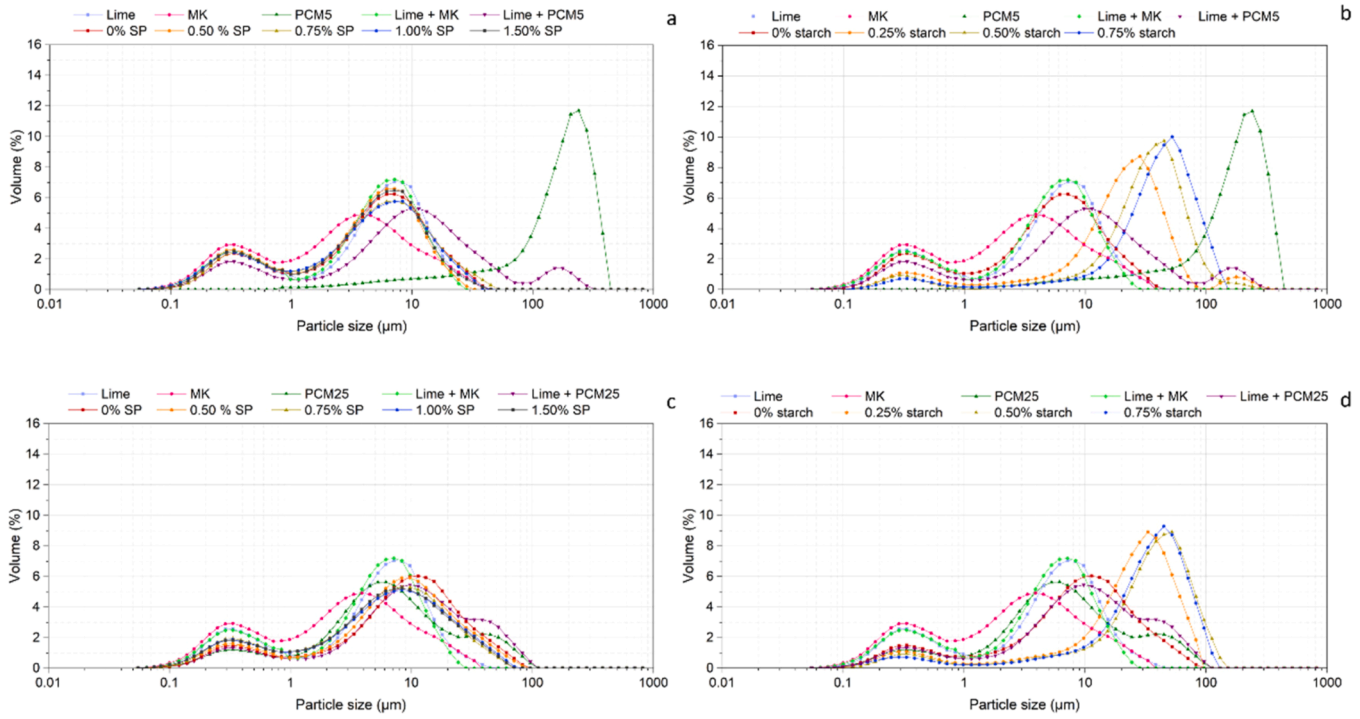

Fig. 3. Particle size distributions of aqueous suspensions of lime and metakaolin containing: (a) PCM5 with increasing dosages of superplasticiser, (b) PCM5 with increasing dosages of starch based additive, (c) PCM25 with increasing dosages of superplasticiser, and (d) PCM25 with increasing dosages of starch based additive.

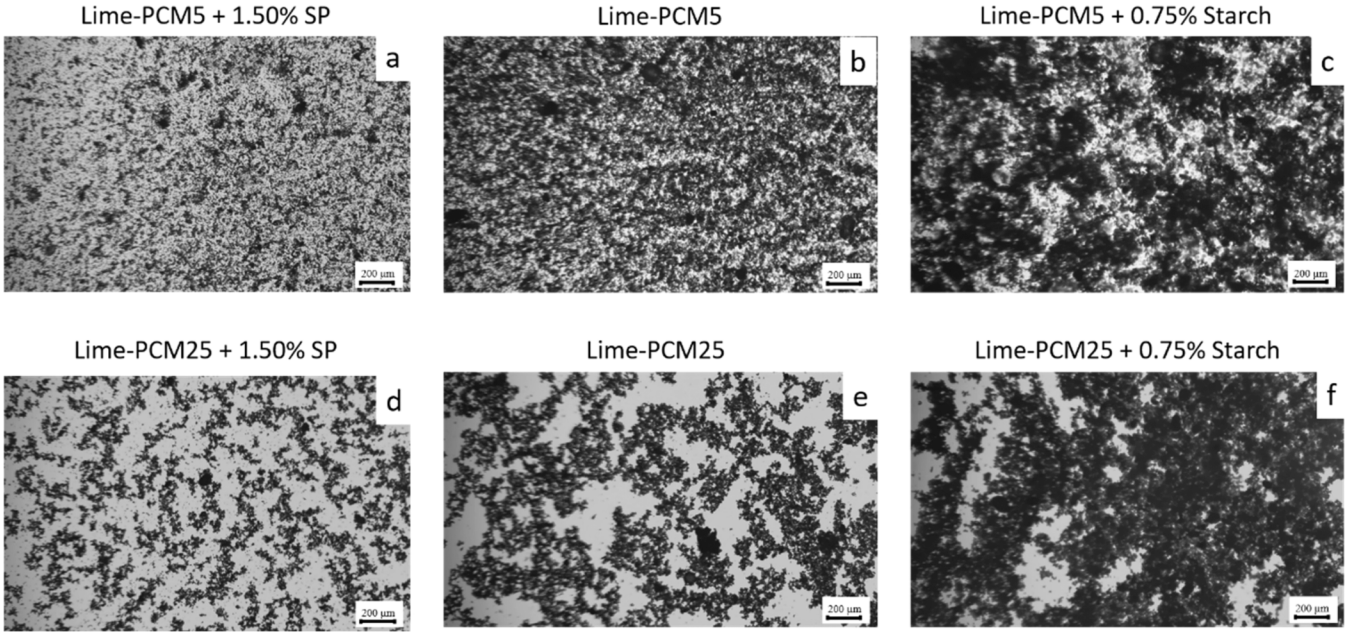

Fig. 4. Optical micrographs of lime-based suspensions containing PCMs and chemical additives (scale bar: 200 μm) (central images are additive-free suspensions): (a-c) PCM5-containing suspensions: (a) with superplasticiser, showing enhanced particle dispersion; (b) without chemical additives; and (c) with starch-based adhesion promoter, exhibiting the formation of larger particle agglomerates. (d-f) PCM25-containing suspensions: (d) with superplasticiser, displaying improved dispersion; (e) without chemical additives; and (f) with starch-based adhesion promoter, characterised by pronounced particle aggregation.

more homogeneous and finely dispersed particle arrangement, consistent with the leftward shifts observed in the granulometric distributions and indicative of enhanced dispersion within the system. In contrast, suspensions containing the starch-based adhesion promoter exhibit visibly larger and more irregular particle assemblages, reflecting the agglomeration effects inferred from the displacement of the particle size distributions towards coarser diameters. These visual features confirm the distinct roles of the two additives and reinforce the interpretation that the PCM particles remain stable while the overall suspension structure is modulated by the dispersing or agglomerating action of the chemical admixtures.

These interactions were further examined by zeta potential measurements to assess surface charge and colloidal stability in the presence of chemical additives. The behaviour of the fully combined systems,

representing the multicomponent environment of the actual mortar formulations, is presented in Fig. 5. These suspensions contain lime, PCM and superplasticiser simultaneously, with metakaolin incorporated where applicable, and the starch derivative is progressively added as titrating agent. Before the addition of any dispersing or stabilizing agents, the suspension exhibits strongly positive zeta potential values, higher than those previously reported for lime-based systems containing microencapsulated phase change materials (PCMs) [19]. In addition to the inherent positive surface charge of portlandite crystals, the alkaline environment promotes the deprotonation of silanol groups on the silica support of the form-stable PCMs. The resulting negatively charged sites are subsequently electrostatically screened by calcium ions present in the lime matrix, thereby contributing to the overall positive zeta potential of the system.

Upon progressive titration with starch, a marked decrease in the zeta potential is observed, reaching values of approximately 90–100 mV, in good agreement with those reported for comparable colloidal systems containing microencapsulated PCMs [19]. This behaviour is attributed to starch-induced flocculation, as evidenced by the increase in particle size and corroborated by optical microscopy. The gradual adsorption of starch onto the surfaces of portlandite crystals alters the interfacial charge balance by reducing the extent of calcium-ion-mediated charge screening, leading to a progressive decrease in the zeta potential. An asymptotic value is ultimately reached, indicating saturation of the adsorption process and stabilization of the interfacial electrostatic conditions. In all formulations, the suspensions maintain a high degree of electrostatic stability, confirming that, even in these more complex systems, all components remain mutually compatible under alkaline conditions.

Taken together, the particle size, optical microscopy and zeta-potential results provide a coherent picture of systems that are highly compatible and electrostatically stable. Neither PCM type nor the presence of metakaolin induces disruptive interactions, and both chemical additives act through predictable charge-compensation mechanisms without compromising stability. Even in the most complex formulations, the suspensions maintain strongly positive zeta potential values and well-defined granulometric profiles, confirming that the combined use of PCMs, superplasticiser and starch derivative is fully compatible with lime-based binders under the alkaline conditions relevant to mortar preparation.

3.2. Optimization of the formulation and fresh state characterization

Building on the detailed assessment of interactions and compatibilities among the additives, PCMs and the lime matrix, the formulation was subsequently refined to optimise the fresh-state behaviour of the renders. Since the addition of PCMs is known to reduce fluidity, promote early-age cracking and impair adhesion to the substrate, the dosages of superplasticizer and adhesion promoter were carefully adjusted to counteract these effects [19]. This optimisation strategy enabled the development of a render formulation with adequate workability, improved cohesiveness and crack-free performance, ensuring its practical applicability. The final optimised composition is presented in Table 2.

For enhanced practical interpretation, the mortar formulations were also converted into kg/m^3 through application of the absolute-volume approach following ASTM C188–17 [66]. The true densities of the dry raw materials were experimentally measured, and the resulting values correspond to theoretical volumetric compositions intended to improve reproducibility and facilitate comparison with more conventional volumetric mix design methodologies (Table 3).

The fresh-state properties of the optimised mortars are summarised in Table 4. The incorporation of PCM resulted in a noticeable increase in consistency, with all PCM-bearing mixtures exhibiting higher flow values than their respective controls. This behaviour reflects the effectiveness of the adjusted superplasticizer dosage in compensating the typical loss of workability associated with PCM addition, ultimately yielding slightly more fluid mortars. Fresh density showed a modest decrease in the PCM-containing formulations, a trend consistent with the slight increase in entrapped air observed in these mixtures. Although

Table 2
Composition of the optimised lime-based mortar mixtures expressed by weight of lime (bwol).

Mixture	PCM5 (% bwol)	PCM25 (% bwol)	SP (% bwol)	Starch (% bwol)	MK (% bwol)	Water (wt %)
CTRL−1	0	0	0.60	0.50	0	25
CTRL−2	0	0	0.75	0.50	20	25
PCM5/0	10	0	0.75	0.50	0	25
PCM5/20	10	0	0.75	0.50	20	25
PCM25/0	0	10	0.75	0.50	0	25
PCM25/20	0	10	0.75	0.50	20	25

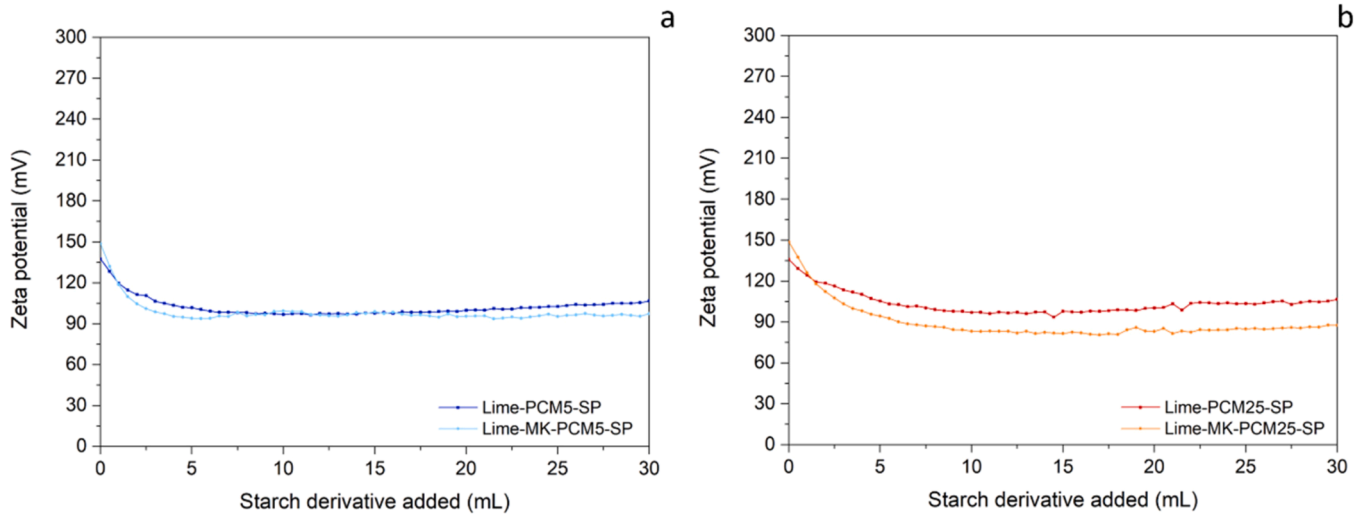

Fig. 5. Zeta-potential evolution of multicomponent suspensions containing lime, superplasticiser and starch derivative with either (a) PCM5 or (b) PCM25, with or without metakaolin.

Table 3
Volumetric mix compositions of the developed laboratory mortars expressed in kg/m^3.

	CTRL−1	CTRL−2	PCM5/0	PCM5/20	PCM25/0	PCM25/20
Hydrated lime	309.12	300.41	299.66	291.54	299.21	291.12
Calcareous sand	1115.40	1083.96	1081.24	1051.96	1079.64	1050.44
Metakaolin	0.00	60.08	0.00	58.31	0.00	58.22
Starch	1.55	1.50	1.50	1.46	1.50	1.46
Superplasticiser	1.85	2.25	2.25	2.19	2.24	2.18
Water	356.13	346.09	345.22	335.87	344.71	335.39
PCM5	0.00	0.00	29.97	29.15	0.00	0.00
PCM25	0.00	0.00	0.00	0.00	29.92	29.11

Table 4
Fresh state results of the optimised mortars.

Mixture	Consistency (mm)	Fresh mortar density (kg/m^3)	Entrapped air (%)	Water retentivity (%)	Qualitative evaluation of rendering (0−3)*
CTRL−1	182	1940	4.3	95.9	3
CTRL−2	175	1943	2.4	95.6	3
PCM5/0	198	1885	6.0	92.4	3
PCM5/20	202	1900	4.0	92.4	3
PCM25/0	199	1875	3.8	93.0	3
PCM25/20	192	1883	4.6	93.2	3

* The qualitative rendering score ranges from degree 3, indicating excellent adhesion with no visible cracks, to degree 0, corresponding to poor adhesion with deep and extensive cracking.

air content rose marginally in most PCM-bearing mortars, the values remained low and did not indicate any negative effect on mixture cohesion or stability. Water retentivity decreased moderately in all PCM-modified formulations, from approximately 96% in the controls to around 92–93%, yet remained sufficiently high to ensure adequate curing conditions and compliance with rendering requirements.

Overall, these results confirm that the optimised formulations achieve appropriate consistency, density, air content and water retention. The adjusted dosages of chemical additives successfully preserved the fresh-state performance of the mortars despite PCM incorporation.

The suitability of the optimised formulations for use as renders was further validated through the qualitative assessment summarised in Table 4. All mixtures achieved the highest score (3), reflecting excellent behaviour during spreading and finishing. The photographs in Fig. 6 illustrate the uniform appearance of the applied layers, characterised by continuous, cohesive surfaces with no visible cracks, detachment or signs of poor adhesion. These observations are consistent with the fresh-state properties discussed previously, confirming that the optimised

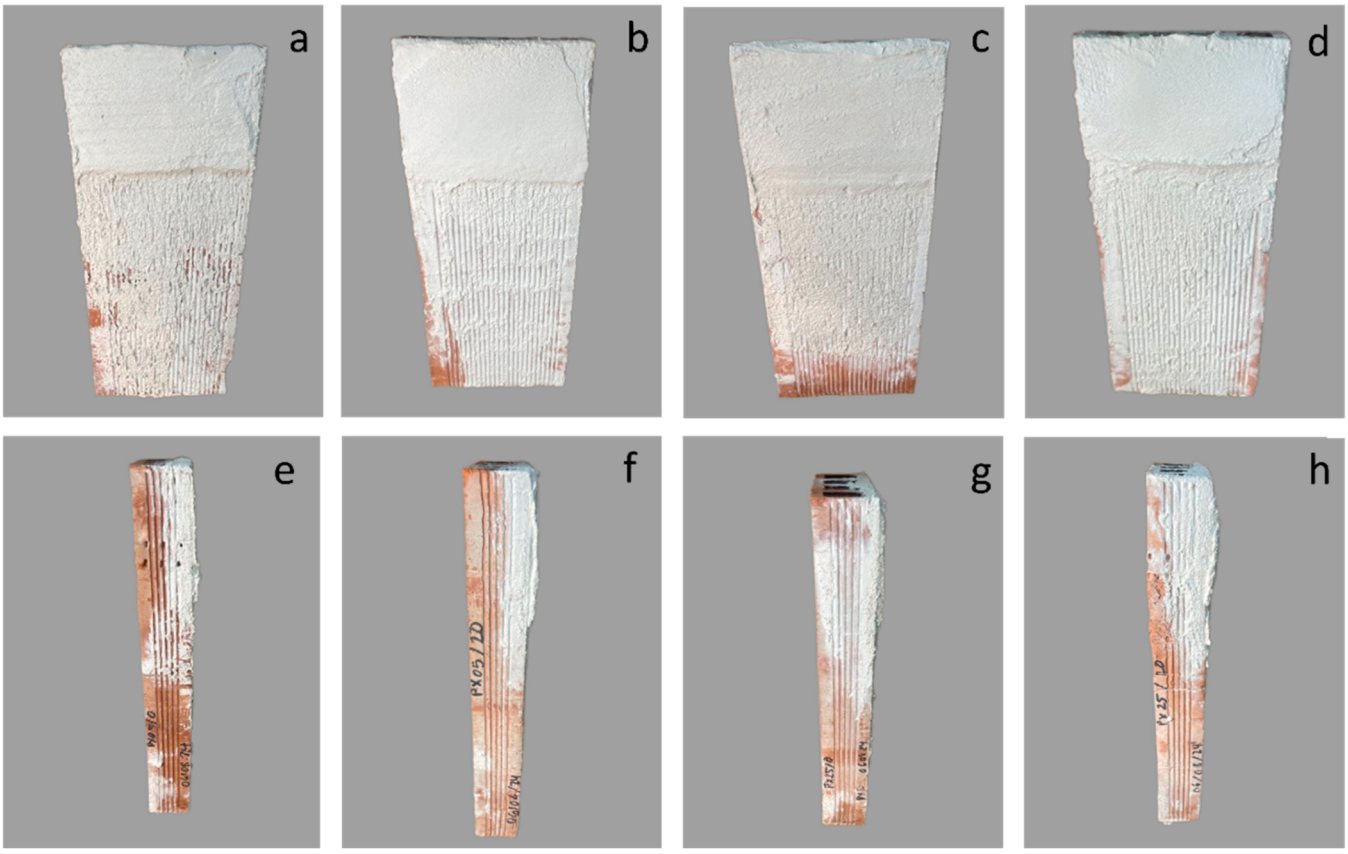

Fig. 6. Rendering performance of the optimised mortars applied on saturated clay bricks. Front views (a-d) and lateral views (e-h) correspond to mixtures PCM5/0, PCM5/20, PCM25/0 and PCM25/20, respectively.

balance between superplasticizer and adhesion promoter provided sufficient fluidity, cohesion and water retention during application. Taken together, the quantitative measurements and visual inspection demonstrate that the PCM-bearing mortars developed in this study meet the practical requirements for lime-based render applications.

3.3. Microstructural assessment

The microstructural assessment first characterised the textural properties of the silica-supported PCMs in their pure form, prior to examining their behaviour within the lime matrix. Establishing the intrinsic porosity, pore-size distribution and surface characteristics of the PCM particles was essential, as these features govern both their interaction with the binder and their thermal performance. Nitrogen adsorption-desorption analysis (BET and physisorption) of the pure form-stable PCMs was therefore carried out to determine the specific surface area and to classify the pore network according to IUPAC criteria [67].

The adsorption-desorption isotherms obtained for PCM5 and PCM25 correspond to a type IV profile (Fig. 7a) with an H3 hysteresis loop (Fig. 7b), as defined by the IUPAC classification [67,68], confirming the mesoporous character expected for a silica matrix loaded with paraffin [60,69–71]. The modest uptake at low relative pressures ($P/P_o < 0.01$) indicates a limited microporous contribution, whereas the gradual increase at intermediate pressures and the sharp rise at high P/P_o reflect the presence of large mesopores and interparticle voids [67]. This behaviour is fully consistent with the porous nature of silica granules in which the paraffin should be retained [60,70,71]. The open and plate-like aggregation typical of silica-derived materials produces slit-shaped pores and interparticle cavities, accounting for both the absence of a distinct capillary condensation step and the pronounced H3 hysteresis observed during desorption [72,73]. Consequently, both PCMs exhibit predominantly mesoporous and partially macroporous structures, characteristic of loosely packed siliceous particles whose pore networks remain accessible after paraffin incorporation [60, 72–75].

Although PCM5 and PCM25 present the same isotherm type, PCM25 consistently adsorbs lower amounts of N_2 across the entire P/P_o range, reflecting its reduced accessible porosity. This behaviour is attributed to the longer chain paraffinic phase in PCM25, which occupies a larger fraction of the silica pore network and therefore decreases the intraparticle porosity available for N_2 adsorption. The lower uptake of PCM25 thus primarily indicates a higher degree of pore filling by the paraffin phase rather than differences in the silica morphology itself.

The BJH pore-size distributions further support these distinctions (Fig. 7c). PCM5 displays a broad pore size range from approximately 2–120 nm, while PCM25 exhibits the same overall range but with systematically lower incremental pore volumes across both the mesoporous and macroporous domains. The dominant mesoporous contribution for PCM5 lies between approximately 3 and 7 nm (30–70 Å), where the incremental pore volume remains nearly constant at around 0.020 cm^3 / g, indicating a broad population of medium-sized intraparticle mesopores (Fig. 7d) [67,70]. These pores represent the internal mesostructure of the silica support and correspond to the intraparticle

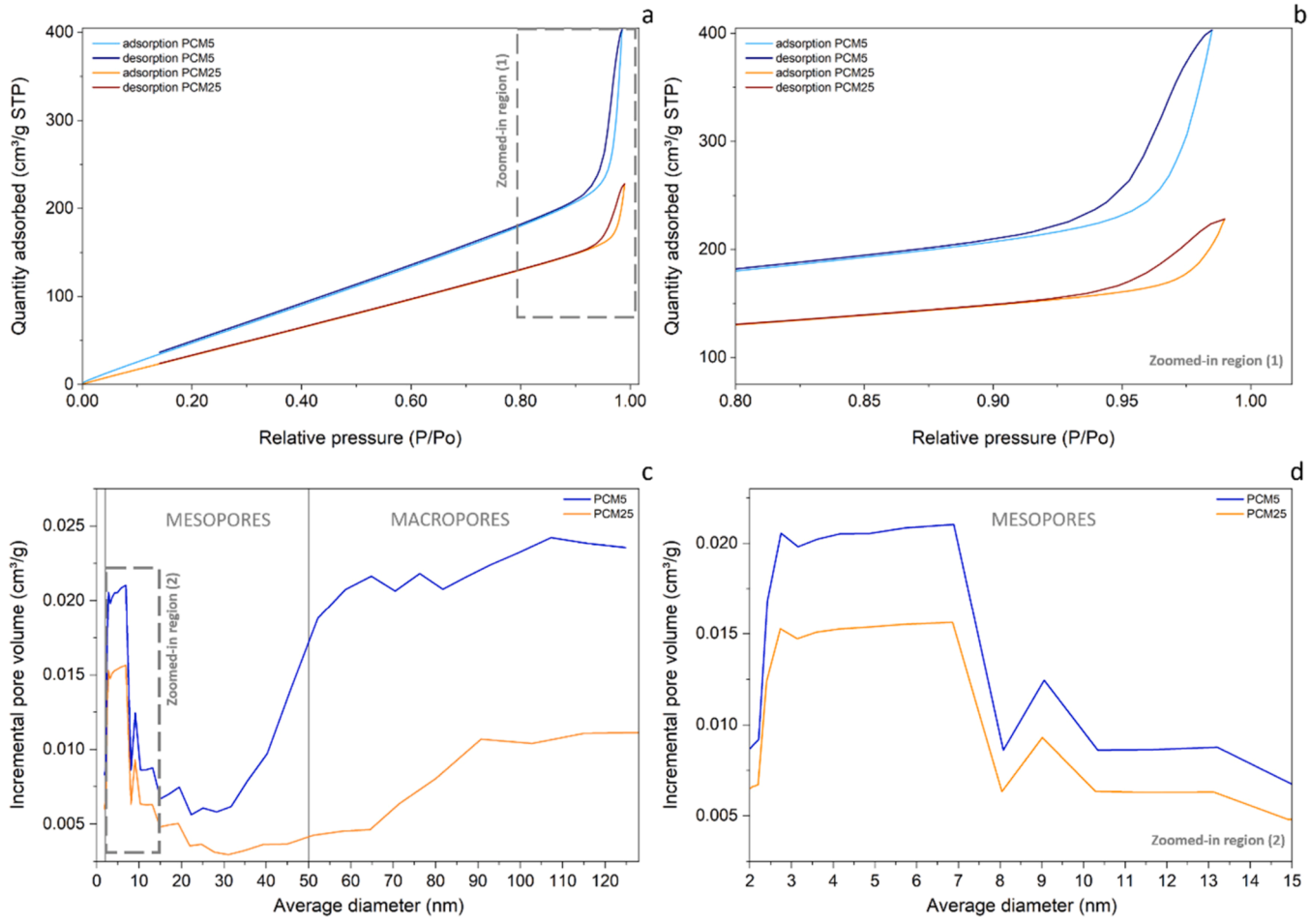

Fig. 7. Physisorption analysis of pure PCMs: (a) N_2 adsorption-desorption isotherms, with a dashed-line box indicating the region selected for magnification; (b) enlarged view of the H3 hysteresis region corresponding to the boxed area in panel (a); (c) BJH pore-size distribution over the full range, including a dashed-line box marking the mesopore domain enlarged in panel (d); (d) enlarged view of the mesopore region.

porosity most relevant to particle-binder interactions after incorporation into the mortar. PCM25 also contains mesopores within this range, but with notably lower incremental values (ca. 0.015 cm^3/g, which represented a 25% reduction), confirming its smaller accessible mesoporous fraction (Fig. 7d).

For both PCMs the incremental pore volume also shows a clear and progressive increase beginning at approximately 35–40 nm and reaching a broad maximum between 60 and 120 nm, reflecting the presence of interparticle voids generated by the packing of silica particles in the dry powder [75]. Taken altogether, the pore size distributions indicate that both PCMs consist of a mesoporous silica network complemented by a secondary contribution of textural porosity arising from particle packing.

The BET surface areas obtained for the two silica-supported PCMs show distinct but expected differences consistent with their textural behaviour. PCM5 exhibited a surface area of 327 m^2/g, whereas PCM25 displayed a lower value of 257 m^2/g. This reduction mirrors the nitrogen adsorption trends observed in the isotherms and is attributed to the longer hydrocarbon chains in the PCM25 paraffin, which occupy a larger fraction of the silica pore volume and therefore decrease the accessible internal surface area. Both materials fall within the expected range for mesoporous silica carriers, and the observed differences reflect the molecular characteristics of the incorporated paraffins rather than changes in the underlying silica framework [59,60].

With the textural properties of the form-stable PCMs established, the analysis proceeded to evaluate how their incorporation affects the pore structure of the lime mortars. Mercury intrusion porosimetry (MIP) was performed on the hardened composites, and the resulting pore-size distribution curves (Fig. 8) reveal clear trends associated with both PCM type and overall mortar composition.

The pore-size distribution curves of the PCM-free mortars (Fig. 8a) exhibit a single dominant capillary peak centred between approximately 0.1 and 2 μm, a characteristic feature of air-lime matrices [76]. CTRL−1 shows its maximum shifted toward slightly larger pore diameters, along with a higher peak intensity, indicating a greater concentration of accessible pores in that range and therefore a coarser pore structure in the absence of metakaolin. In contrast, CTRL−2 presents a peak located at smaller pore sizes and with lower intensity, consistent with a finer and less voluminous pore population. This behaviour aligns with the well-documented pore-refining effect of metakaolin, which promotes the formation of pozzolanic reaction products capable of filling and narrowing the pore network [24,76–78].

The mortars incorporating PCM5 exhibit pore-size distributions closely matching those of their respective reference binders (Fig. 8b). PCM5/0 displays a dominant peak nearly coincident with that of CTRL−1, with only a slight shift toward smaller pore diameters, likely reflecting a minor filler-like effect of the PCM particles. Similarly, PCM5/20 shows a distribution very similar to CTRL−2, again with a minimal leftward displacement of the main peak. Comparison of the two PCM5-bearing mortars highlights the effect of metakaolin: PCM5/20

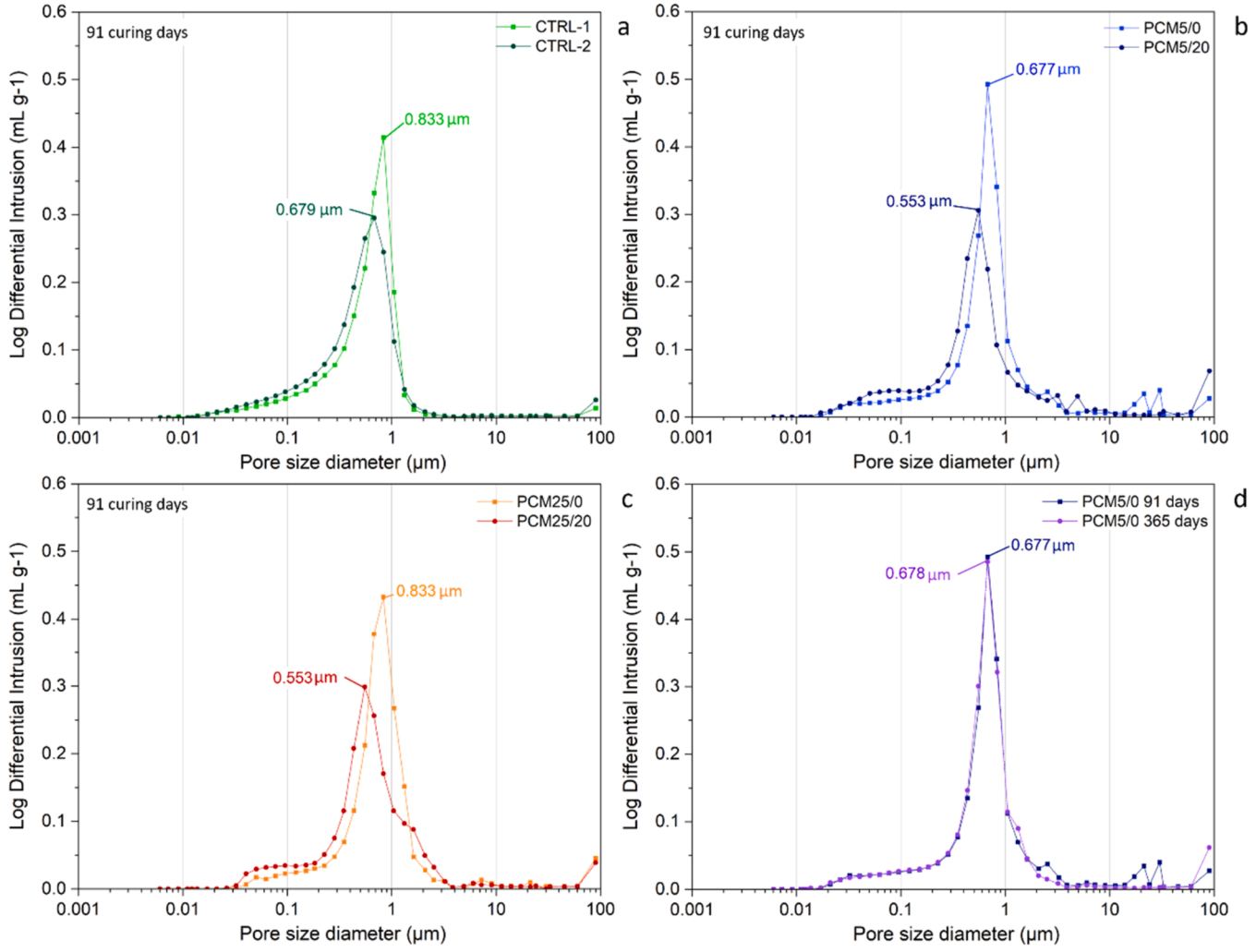

Fig. 8. Pore size distribution curves of lime mortars obtained by MIP: (a) PCM-free mortars at 91 curing days, (b) PCM5-bearing mortars at 91 curing days, (c) PCM25-bearing mortars at 91 curing days and (d) PCM5-bearing mortars at 91 and 365 curing days.

develops a subtle shoulder below 0.1 μm, which may correspond to fine pozzolanic reaction products [76]. Furthermore, the small secondary intrusions present in the coarse-pore region of PCM5/0 are markedly reduced in PCM5/20, reinforcing the pore-refining action associated with metakaolin [76,78].

The pore-size distributions of the PCM25-containing mortars (Fig. 8c) closely resemble those of their respective reference binders but with a slightly more pronounced shift of the main peak toward smaller pore diameters, particularly in PCM25/20. As observed in PCM5, this subtle leftward shift may reflect a minor filler-like contribution from the silica-supported PCM. A direct comparison of PCM25/0 and PCM25/20 shows that PCM25/20 exhibits a slightly smaller peak diameter and a faint shoulder below 0.1 μm, features typically associated with the formation of fine pores linked to pozzolanic reaction products in MK-modified lime mortars [76].

A comparison of the pore-size distributions at 91 and 365 days (Fig. 8d; additional curves provided in Supplementary Material Figure S3) shows that the pore structure of the mortars remained essentially stable over time. For all mixtures, both the position and intensity of the dominant peak were virtually unchanged, indicating that the characteristic pore-size distribution established at early-medium ages is largely preserved after extended curing. Only minor differences were noted in the coarse-pore region, where small secondary intrusions around 20–30 μm tend to diminish or become less pronounced at 365 days. This slight attenuation may reflect ongoing matrix densification associated with carbonation, although its magnitude is limited. Overall, the long-term evolution of the pore network is minimal, confirming that neither PCM incorporation nor MK addition induces significant changes in the porous structure during curing.

All things considered, the strong similarity between the PCM-bearing mortars and their PCM-free references indicates that the lime matrix accommodates the silica-supported PCMs without generating disruptive alterations in the pore network. This is a particularly advantageous result, as it demonstrates that the inclusion of form-stable PCMs does not compromise the porous structure responsible for vapour transport, mechanical integrity and long-term compatibility in lime-based materials.

To further verify the microstructural observations inferred from mercury intrusion porosimetry, SEM imaging was performed. The morphology of the silica-supported PCMs in their pure form is shown in Fig. 9. PCM5 (Fig. 9a) and PCM25 (Fig. 9b) both exhibit irregular granules with predominantly ellipsoidal shapes and a broad range of particle sizes. Their surfaces appear rough and finely textured, consistent with the mesoporous structure identified by physisorption analysis.

The microstructural features of the lime mortars incorporating silica-supported PCMs are shown in Fig. 10. In all cases, the matrices exhibit a compact and continuous structure, with no evidence of microstructural discontinuities or heterogeneities. The overall morphology appears homogeneous and is fully consistent with the MIP results, which indicated that the PCM incorporation caused only minimal changes in total porosity and pore-size distribution. The absence of cracks, gaps, or interfacial voids suggests that the silica-supported PCMs are well integrated within the lime matrix, preserving its integrity and structural cohesion. The mortars containing metakaolin (PCM5/20 and PCM25/20, Fig. 10b and Fig. 10d) show slightly denser textures, although the effect is lenient, consistent with the limited extent of pozzolanic reaction inferred from the MIP analysis.

The morphological characteristics of the silica-supported PCMs shown in Fig. 9 help explain why these particles cannot be readily distinguished within the lime matrices observed in Fig. 10. The ellipsoidal silica granules possess rough and irregular surfaces that closely resemble the textural features of the surrounding lime matrix, making visual differentiation between the PCM particles and binder challenging. Moreover, the intimate contact between the PCM granules and the lime mortar produces a continuous microstructure with no visible contrast or interfacial boundaries. This morphological compatibility aligns with the compact appearance and absence of discontinuities previously noted, confirming that the silica-supported PCMs are well accommodated within the matrix and do not disrupt its structural integrity.

To further substantiate this interpretation, EDS elemental mapping was performed (Fig. 11). The carbon, calcium and oxygen maps (Fig. 11b-d) show a uniform distribution of the binder phases, whereas the silicon map (Fig. 11e) and its corresponding quantitative distribution (Fig. 11f) reveal a homogeneous dispersion of the silica-rich domains associated with the PCMs, with some areas showing a slightly higher accumulation (purple areas) corresponding to somewhat larger PCM particles, in line with the polydispersity of this material observed in Fig. 9. The close spatial correspondence among these elemental signals confirms that the silica-supported PCMs are evenly distributed throughout the lime matrix, with no evidence of clustering or segregation. Taken together, these results reinforce the conclusions drawn from MIP and SEM, demonstrating that the incorporation of form-stable PCMs preserves the compactness, uniformity and continuity of the lime microstructure.

3.4. *Compressive strength resistance*

The evolution of compressive strength with curing age for all mixtures is presented in Fig. 12. In every case, mortars containing silica-supported PCMs developed higher compressive strength than their corresponding PCM-free references. This behaviour contrasts with much of the existing literature on form-stable PCMs supported on siliceous carriers, where reductions in compressive strength are frequently reported when these materials are incorporated without appropriate optimisation of the mix design, particularly when water demand is not adequately controlled [79–83]. In the present study, however, all formulations were prepared with a constant water content and were specifically adjusted to ensure adequate workability, cohesive spreading and crack-free application as renders. Under these controlled conditions,

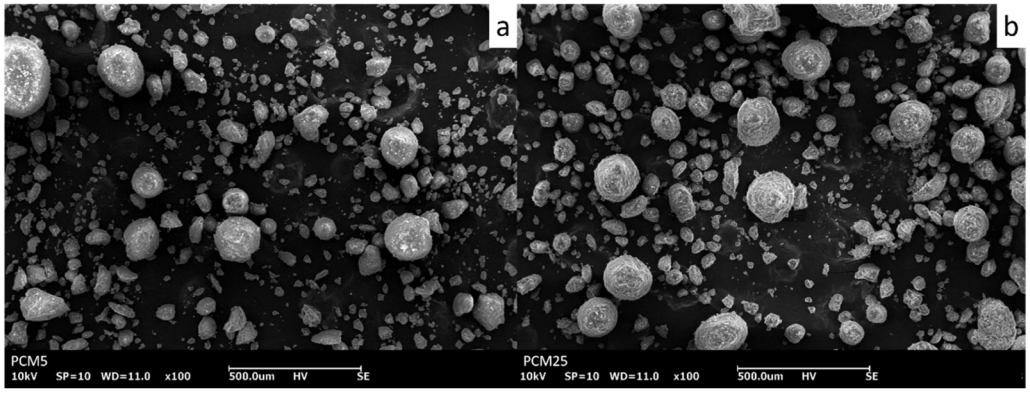

Fig. 9. SEM images of pure PCMs: (a) PCM5 and (b) PCM25.

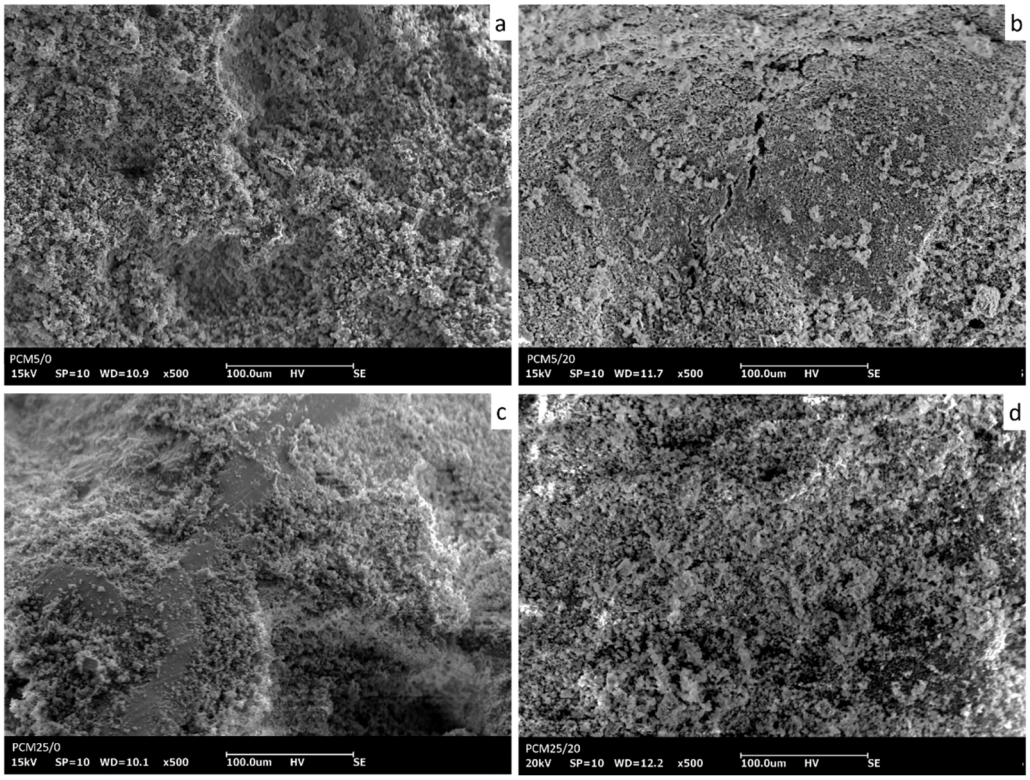

Fig. 10. SEM images of PCM-bearing mortars: (a) PCM5/0, (b) PCM5/20, (c) PCM25/0 and (d) PCM25/20.

the silica carriers acted as mechanically robust inclusions whose intrinsic rigidity and particle integrity allowed them to be effectively embedded within the lime matrix (as confirmed by SEM, Fig. 11), contributing to a measurable enhancement in compressive strength.

With regard to curing age, all mixtures showed a marked increase in compressive strength between 28 and 91 days, followed by comparatively stable values at later ages (Fig. 12). This trend indicates that majority of the mechanical development occurs within the first three months, after which the mortars approach a steady state. This behaviour is fully consistent with the MIP results, where pore-size distributions showed minimal variation between 91 and 365 days (Fig. 8d and Figure S3), suggesting that the microstructure had largely stabilised during this period, thus limiting strength development.

Comparison of MK-free and MK-bearing mixtures shows that the inclusion of metakaolin generally leads to slightly higher strengths (CTRL−2 vs CTRL−1, PCM5/20 vs PCM5/0, PCM25/20 vs PCM25/0), although the improvements remain modest rather than substantial (Fig. 12). This outcome is compatible with the limited microstructural differences identified by MIP and SEM between mixtures with and without metakaolin (Fig. 8 and Fig. 10), and can be explained by the curing and mix-design conditions used in this study, which are not optimal for extensive pozzolanic reaction. According to the literature, lime-metakaolin systems achieve their greatest mechanical enhancement when MK contents approach approximately 25 wt% and when curing is performed under high moisture conditions (typically around 95 ± 5% R.H.), which promote sustained pozzolanic activity [24,84]. In contrast, the mortars evaluated here were produced with a fixed mixing water content of 25 wt% (for consistency across formulations), cured at a comparatively lower relative humidity of 60 ± 5% R.H., and incorporated 20% MK bwol, conditions that limit the extent of pozzolanic reaction and therefore explain the modest strength gains observed.

Taken together, these findings highlight that thorough optimization of the mortar formulation is essential for the successful incorporation of silica-supported, form-stable PCMs. When water content, chemical additive dosage, mineral admixtures and fresh-state performance are rigorously controlled, these inclusions can be integrated into lime mortars without any detrimental effects on mechanical behaviour. On the contrary, the resulting composites exhibit enhanced compressive strength, confirming that the rigid siliceous carriers can be effectively accommodated within the lime matrix without compromising structural integrity. This outcome underscores the importance of mix-design optimisation when implementing functional additives in lime-based materials and demonstrates the feasibility of achieving mechanical robustness while simultaneously introducing latent-heat storage capacity.

3.5. *Thermal behaviour*

Following the microstructural and mechanical evaluation, the thermal response of the mortars was assessed. Fig. 13 shows the thermal conductivity (λ) values obtained at several temperatures covering both the solid and liquid states of the PCM. The control mixtures (CTRL−1 and CTRL−2) exhibit λ values between 0.33 and 0.40 W/m·K, consistent with the typical range reported for lime-based mortars [14,17,24]. The mortars incorporating silica-supported PCMs display slightly lower conductivities, generally between 0.31 and 0.38 W/m·K, with the largest reduction observed for PCM25/20 (ca. 0.31 W/m·K). This decrease remains moderate and aligns with the microstructural evidence from MIP and SEM, which showed that PCM addition does not significantly modify the pore network of the lime matrix. The close similarity between the pore-size distributions of PCM-bearing mixtures and their corresponding references confirms that the lime matrix accommodates the PCMs without inducing major porosity changes; thus, variations in λ are unlikely to stem from microstructural alterations.

Instead, the observed reductions in thermal conductivity can be attributed primarily to the intrinsically low λ values of both components of the form-stable system: the paraffinic PCM and the porous silica support, each characterized by inherently low conductivity [85–88]. This interpretation is consistent with manufacturer specifications, which report λ values on the order of 0.1–0.2 W/m·K for the silica-supported

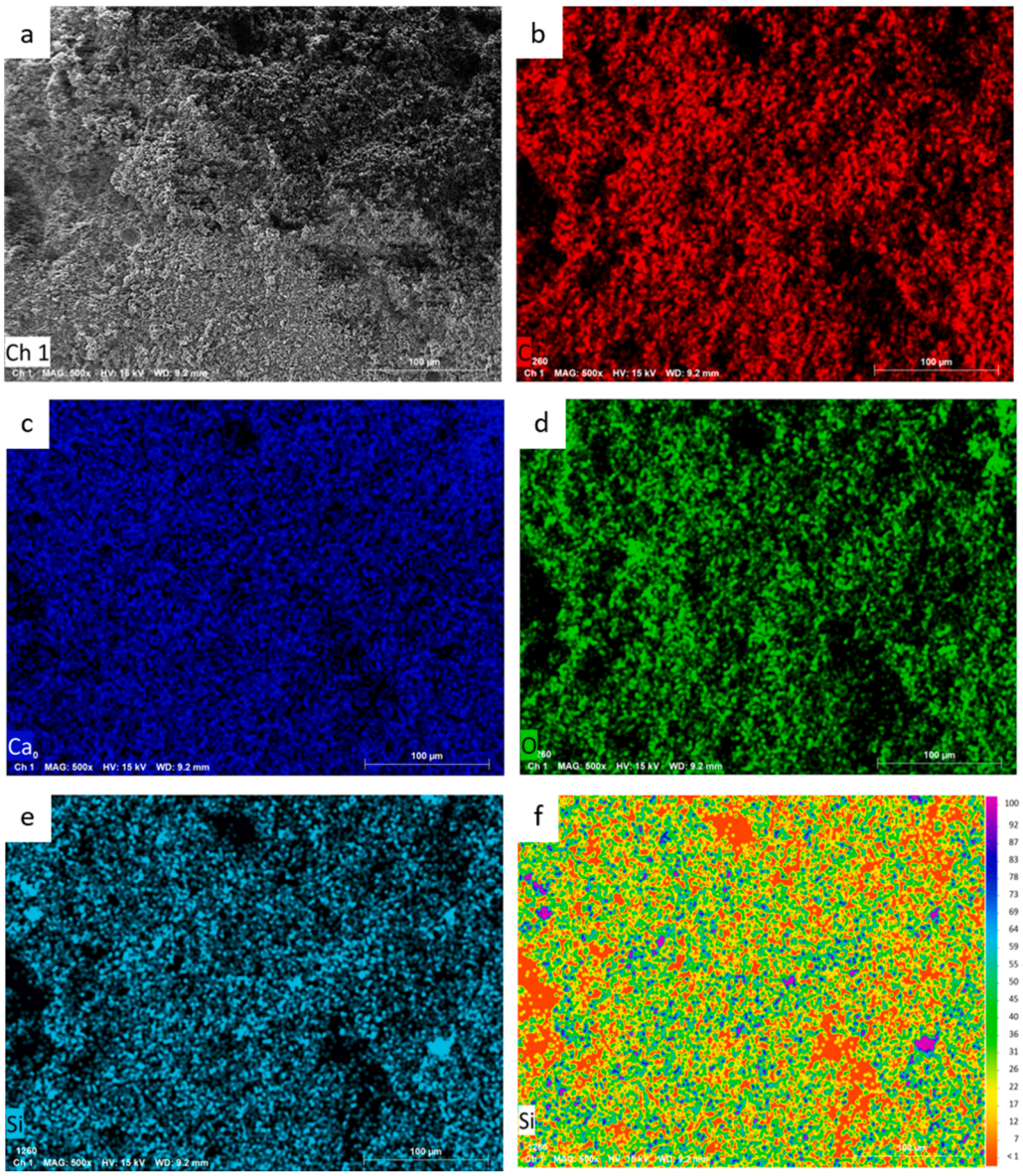

Fig. 11. EDS elemental mapping of PCM25/0: (a) SEM micrograph of the analysed area; (b) carbon map; (c) calcium map; (d) oxygen map; (e) silicon map; (f) quantitative Si distribution map. The homogeneous presence of Si throughout the matrix confirms the even dispersion of the silica-supported PCM within the lime mortar.

PCMs. Their incorporation therefore introduces finely dispersed, low-conductivity inclusions that marginally increase the overall thermal resistance while preserving matrix continuity. Additionally, the slight leftward shift observed in the pore-size distributions of PCM5 and PCM25 mixtures (Fig. 8) may contribute a small additional reduction in λ [89].

The nearly constant conductivity observed across the tested temperatures confirms that the thermal performance of the mortars remains predictable under ordinary environmental conditions (Fig. 13). Importantly, the presence of the PCM does not produce anomalies or discontinuities around the melting interval, demonstrating that the silica-supported PCMs act as thermally stable and well-integrated inclusions that do not disrupt conductive pathways.

Overall, the incorporation of silica-supported form-stable PCMs results in a controlled and beneficial reduction in thermal conductivity while maintaining sufficient heat-flow capacity within the matrix. This balance is essential for effective latent-heat storage: if the matrix were overly insulating, heat transfer to the PCM would be hindered, reducing its thermal activation. The measured conductivities therefore represent an optimal compromise between insulation and heat transfer, enabling efficient PCM activation and reinforcing the suitability of these mortars for energy-responsive building envelopes and passive indoor temperature regulation.

The thermal behaviour of the phase change materials was analysed by DSC in order to characterise their latent heat storage and release capacity and to confirm the reversibility of their phase transitions. The corresponding DSC thermograms are shown in Fig. 14, while the main phase-change parameters, including onset, peak and endset transition temperatures and enthalpy values, are summarised in Table 5.

Both PCMs exhibited sharp melting and crystallization peaks (Fig. 14), confirming the reversibility of their phase transitions. The low-temperature PCM (PCM5) displayed enthalpy values of approximately 75 J/g, whereas the high-temperature PCM (PCM25) reached values close to 93 J/g, indicating a higher latent heat storage and release potential. This difference cannot be attributed to variations in paraffin content, as the thermogravimetric analysis curves of PCM5 and PCM25 (Supplementary Material, Figure S4) show nearly identical mass-loss profiles up to around 300 °C, corresponding to the degradation of the

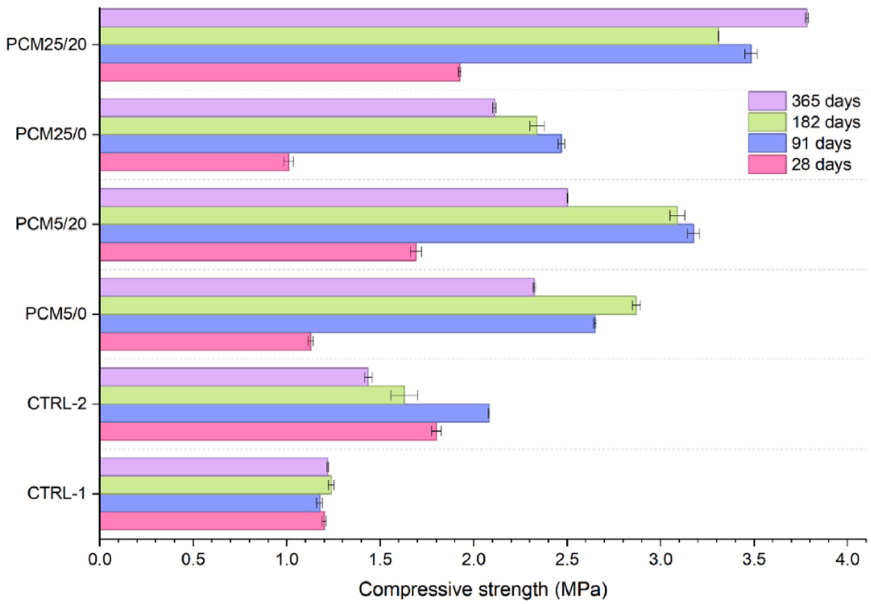

Fig. 12. Compressive strength of lime-based mortars at 28, 91, 182 and 365 days of curing.

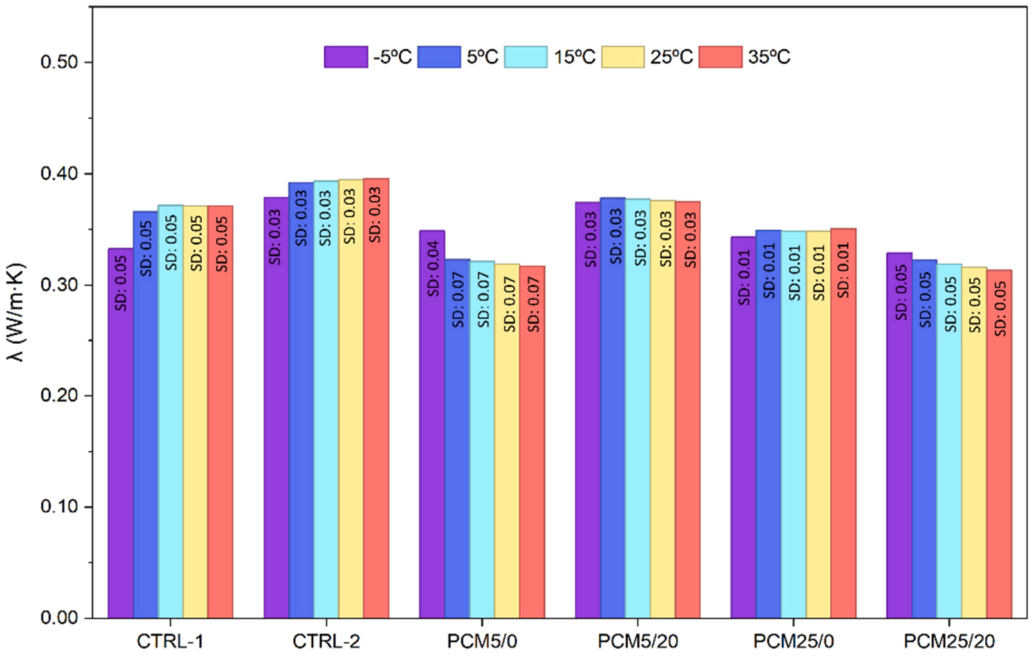

Fig. 13. Thermal conductivity (λ) of lime mortars with and without silica-supported PCMs measured at −5 °C, 5 °C, 15 °C, 25 °C, and 35 °C. SD values correspond to the standard deviation of replicate measurements.

paraffinic phase, as well as similar residual masses associated with the silica support [60]. Instead, the difference is more likely related to the intrinsic thermal behaviour of the paraffinic hydrocarbons composing each PCM. Longer-chain paraffins generally have higher melting temperatures and larger enthalpies of melting, as increased molecular length enhances van der Waals interactions and crystalline packing within the solid phase [90,91]. Thus, the higher melting temperature of PCM25 suggests a predominance of longer-chain alkanes, consistent with the greater enthalpy observed in its DSC curve.

Additionally, PCM25 exhibited two distinct peaks during both melting and crystallization (Fig. 14). This behaviour can be ascribed to solid-solid transitions occurring within the paraffinic phase during heating and cooling, and/or to compositional heterogeneity arising from alkanes of slightly different chain lengths [92–94]. Accordingly, the enthalpy values reported in Table 5 correspond to the combined area of both peaks, whereas the temperatures listed refer to the primary melting and crystallization events, which represent the dominant phase transitions governing the principal thermal storage behaviour and practical functional applicability of the PCM, while the secondary peaks constitute supplementary lower-energy transitions.

Regarding the thermal activation intervals of the evaluated PCMs, PCM5 exhibited a melting interval extending approximately from 2 °C to 13 °C, with crystallization occurring between 4 °C and −8°C, whereas PCM25 displayed substantially higher operational ranges, with the principal melting event occurring between 22°C and 33 °C and crystallizing between 22°C and 10 °C. These transition intervals confirm the

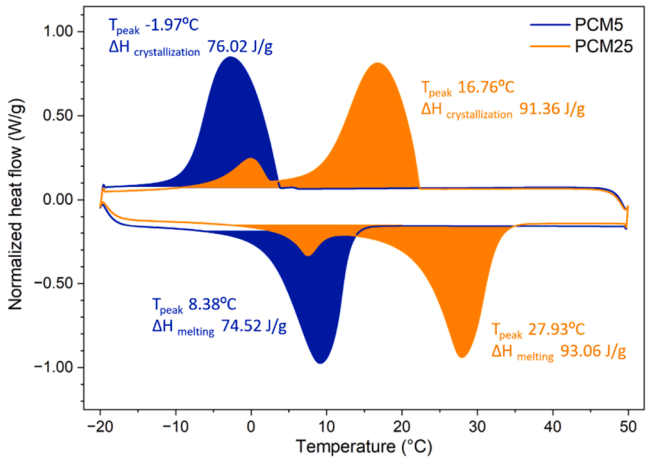

Fig. 14. DSC thermograms of pure PCMs.

fundamentally different activation domains of both PCMs. PCM25 is more directly associated with thermal regulation strategies targeting conventional building comfort ranges, particularly in mitigating overheating and moderating indoor temperature fluctuations. In contrast, PCM5, while less directly aligned with traditional indoor comfort applications, provides valuable insight into the behaviour of lower-transition-temperature form-stable PCMs and hold potential for mitigating lower-temperature fluctuations, broader climatic applications, or future tailored and multi-PCM design strategies aimed at expanding the effective thermal regulation range of lime-based materials.

When compared with microencapsulated paraffinic PCMs commonly used in building materials, the latent-heat values obtained for the silica-supported PCMs fall within the lower end of the typical range reported in the literature. Microencapsulated paraffins generally exhibit melting and crystallization enthalpies between 80 and 200 J/g, depending on the paraffin core, encapsulation efficiency, and shell composition [24,95,96]. Although positioned towards the lower bound of this interval, the silica-supported PCMs still demonstrate a latent-heat capacity sufficient to provide effective thermal response, with an expected potential for energy-efficiency improvement comparable to mortars containing microencapsulated paraffins.

Alongside their latent-heat capacity, the ability of form-stable PCMs to retain the paraffinic phase within the porous silica matrix when the PCM is in the molten state is a key aspect for their practical applicability. To verify this behaviour, complementary leakage tests were performed on PCM5 and PCM25 at 40 °C and 75 °C, both temperatures being well above their respective melting points (Fig. 15). No evidence of paraffin

Table 5
Melting and crystallization parameters of PCMs.

	Melting				Crystallization			
	T_m (°C)	$T_{m,\ onset}$ (°C)	$T_{m,\ endset}$ (°C)	ΔH_m (J/g)	T_c (°C)	$T_{c,\ onset}$ (°C)	$T_{c,\ endset}$ (°C)	ΔH_c (J/g)
PCM5	8.38 ± 0.01	1.81 ± 0.01	13.32 ± 0.01	74.52 ± 0.02	−1.97 ± 0.04	3.68 ± 0.01	−8.36 ± 0.01	76.02 ± 0.01
PCM25	27.93 ± 0.03	21.97 ± 0.01	32.59 ± 0.01	93.06 ± 0.02	16.76 ± 0.01	22.31 ± 0.01	9.91 ± 0.01	91.36 ± 0.09

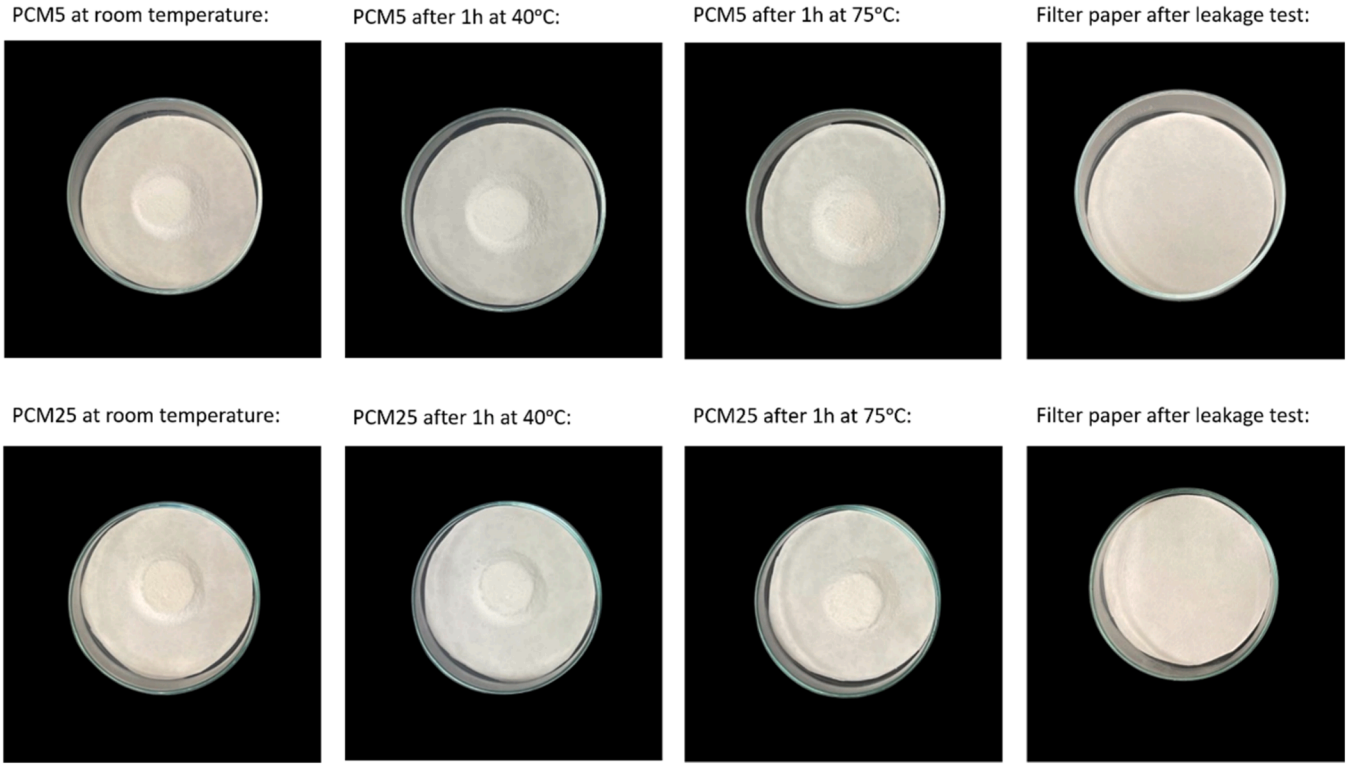

Fig. 15. Qualitative leakage assessment of PCM5 (top row) and PCM25 (bottom row) at different temperatures: samples at room temperature, after 1 h at 40 °C, after 1 h at 75 °C, and corresponding filter substrates after testing.

release was observed under any of the tested conditions: the filter substrates exhibited no halos, wetting marks or other visual indications of leakage. Consistently, gravimetric measurements of the filter papers before and after the tests showed no mass variation, confirming that both silica-supported PCMs effectively retain the paraffinic phase within the porous matrix even when fully molten (Fig. 15).

Lastly, to assess the ability of the PCM-containing mortars to moderate temperature fluctuations under realistic operating conditions, the samples were subjected to controlled heating-cooling cycles between 50 °C and −10 °C in the hotbox configuration. This temperature window was selected to ensure that both PCMs (PCM5 and PCM25) undergo complete melting and crystallization during each cycle, while also representing a plausible range that lime-based renders may experience in service.

Fig. 16a illustrates the temperature evolution of the climatic chamber, the PCM-free mortar (CTRL−2), and the PCM25/20 mortar over four consecutive cycles, as an example. Across all cycles, the PCM-enhanced mortar consistently displays reduced temperature swings compared with the reference, demonstrating a clear buffering effect during both heating and cooling. This behaviour is emphasised in the zoomed-in views: during heating (Fig. 16b), the PCM-containing mortar reaches lower peak temperatures as the PCM absorbs heat during melting; conversely, during cooling (Fig. 16c), it remains comparatively warmer due to heat release upon crystallization. Together, these observations provide a clear qualitative demonstration of the thermal moderation achieved through PCM incorporation.

Quantitative analysis of the peak temperatures provides a clearer measure of this buffering capacity. As summarised in Table 6, all PCM-modified mortars reduced the maximum temperatures reached during heating and increased the minimum temperatures recorded during cooling. The PCM5- and PCM25-bearing mortars exhibited comparable levels of thermal moderation, with slightly lower values for the PCM5 mixtures. PCM5/0 and PCM5/20 lowered peak heating temperatures by 0.6 °C and 0.9 °C, respectively, and reduced cooling drops by up to 0.8 °C. The PCM25 mixtures showed marginally higher moderation, with PCM25/20 reducing heating peaks by up to 1.1 °C and increasing minimum cooling temperatures by 0.8 °C. This trend is consistent with the slightly higher latent heat of PCM25 identified by DSC analysis of the pure PCMs. Overall, these results confirm that both PCMs effectively attenuate thermal fluctuations under dynamic conditions, with PCM25 providing a modestly enhanced buffering effect.

Beyond peak temperatures, the overall temperature moderation

Table 6
Average ΔT at the maximum heating peaks and at the minimum cooling peaks.

Mixture	ΔT_{max} heating (°C)	$\lvert\Delta T_{min}\rvert$ cooling (°C)
PCM5/0	0.6 ± 0.1	0.2 ± 0.1
PCM5/20	0.9 ± 0.1	0.8 ± 0.1
PCM25/0	0.9 ± 0.1	0.3 ± 0.1
PCM25/20	1.1 ± 0.1	0.8 ± 0.1

Table 7
Maximum ΔT during heating and cooling phases.

Mixture	Heating maximum ΔT (°C)	Cooling maximum |ΔT| (°C)
PCM5/0	1.7 ± 0.1	0.3 ± 0.1
PCM5/20	1.9 ± 0.1	1.0 ± 0.2
PCM25/0	2.0 ± 0.1	1.0 ± 0.1
PCM25/20	2.1 ± 0.1	1.5 ± 0.1

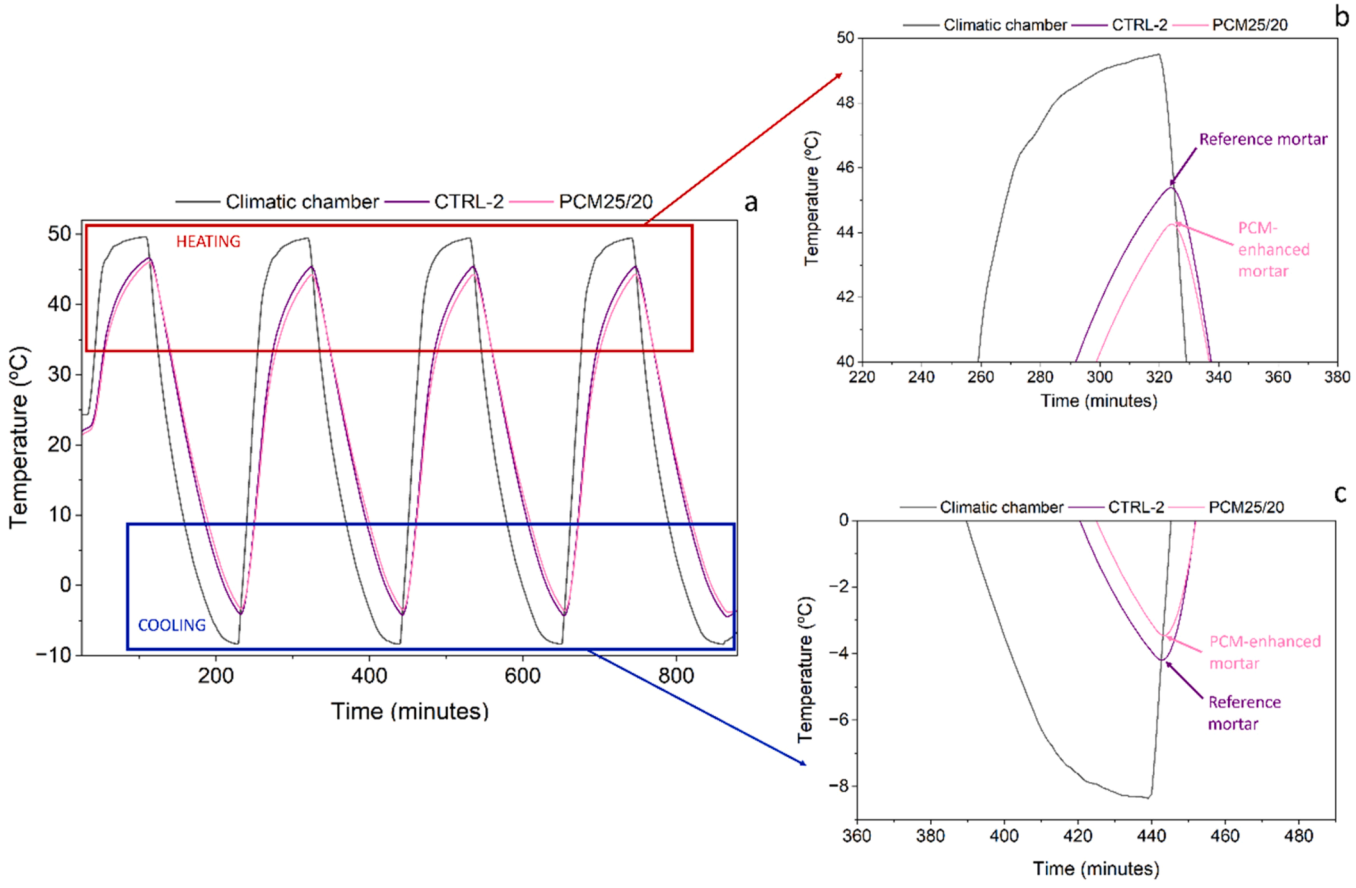

Fig. 16. Temperature evolution during hotbox testing for the PCM25/20 mortar and the reference mortar (CTRL−2): (a) overall temperature response, (b) detail of the heating phase, and (c) detail of the cooling phase, illustrating the thermal buffering effect provided by the PCM.

across the full heating and cooling stages further reinforces these trends. As shown in Table 7, the maximum temperature differences recorded over the entire heating phases demonstrate that both PCM systems effectively smooth the thermal response of the renders. The PCM5 mixtures moderated the heating curve by 1.7–1.9 °C, whereas the PCM25 mixtures achieved reductions of up to 2.1 °C, consistent with their higher latent heat. A similar pattern was observed during cooling, where the PCM-enhanced mortars mitigated the temperature drop by values ranging from 0.3 °C in PCM5/0–1.5 °C in PCM25/20. These results show that the contribution of the latent heat is sustained not only at the temperature extremes but throughout the entire thermal cycle, with PCM25/20 exhibiting the strongest and most persistent temperature-smoothing effect.

The overall thermal buffering achieved during the heating-cooling cycles was quantified by integrating the temperature differences relative to the PCM-free mortar (CTRL) over time. This integral provides an estimate of the net energy absorbed and released by each formulation, thereby capturing the cumulative buffering effect of the PCM throughout the entire cycle [16]. By examining the area enclosed by the ΔT curves (Fig. 17), it is possible to assess how effectively each mortar stores and returns thermal energy and, consequently, to evaluate its potential contribution to improving energy efficiency under fluctuating temperature conditions. The corresponding values for all mixtures are reported in Table 8.

The integral quantifies the extent to which each mortar deviates from the thermal trajectory of the control sample, capturing the overall capacity of the incorporated PCM to moderate temperature variations over time. As shown in Table 8, all PCM-containing mortars exhibited clear and measurable deviations from the reference curve, reflecting their ability to absorb and release heat during the imposed thermal cycles. The PCM5 mixtures yielded values on the order of 2.1×10^4 to 3.9×10^4 °C·s/m^2, whereas the PCM25 mortars reached even higher deviations, up to 4.5×10^4 °C·s/m^2. These results confirm that both PCMs actively contribute to smoothing the thermal response of the lime render under dynamic conditions.

What is especially noteworthy is that these improvements occur despite the very low PCM content of the mortars. Even at such modest dosages, the silica-supported PCMs provide a clear and measurable enhancement in thermal performance, highlighting their potential to significantly improve energy efficiency in real construction scenarios. Moreover, the incorporation of PCMs with distinct transition temperatures broadens the potential applicability of these systems across wider thermal activation ranges, opening new possibilities for the future optimization of tailored thermal buffering strategies. Within this context, the present results establish a robust foundation for future studies under more specific climatic and operational temperature scenarios, where the relative suitability of each PCM formulation may be further refined according to targeted environmental demands. Such progression may additionally facilitate the development of climate-adapted mortars and more advanced multi-PCM or cascade systems capable of extending the active thermal regulation range of building materials.

Table 8
Relative energy exchanged calculated by the integral of temperature variation versus time.

Mixture	Relative energy exchanged (°C·s/m^2)
PCM5/0	$2.1 \cdot 10^4$
PCM5/20	$3.9 \cdot 10^4$
PCM25/0	$3.6 \cdot 10^4$
PCM25/20	$4.5 \cdot 10^4$

3.6. Durability and cyclability

The durability assessment under freeze-thaw cycling and salt attack, summarised in Table 9 and illustrated in Fig. 18, revealed clear differences between the control mortars and the PCM-enhanced mixtures. The weakest performance was observed in CTRL−1, which failed abruptly after only five freeze-thaw cycles and reached a damage score of 10, indicating complete disintegration. CTRL−2 performed better, withstanding 28 cycles before exhibiting extensive cracking and mass loss, reflected in a final score of 9 and the steep decline in its weight-change profile (Fig. 18b). In contrast, all PCM-containing mortars completed the full sequence of 28 cycles with comparatively limited deterioration

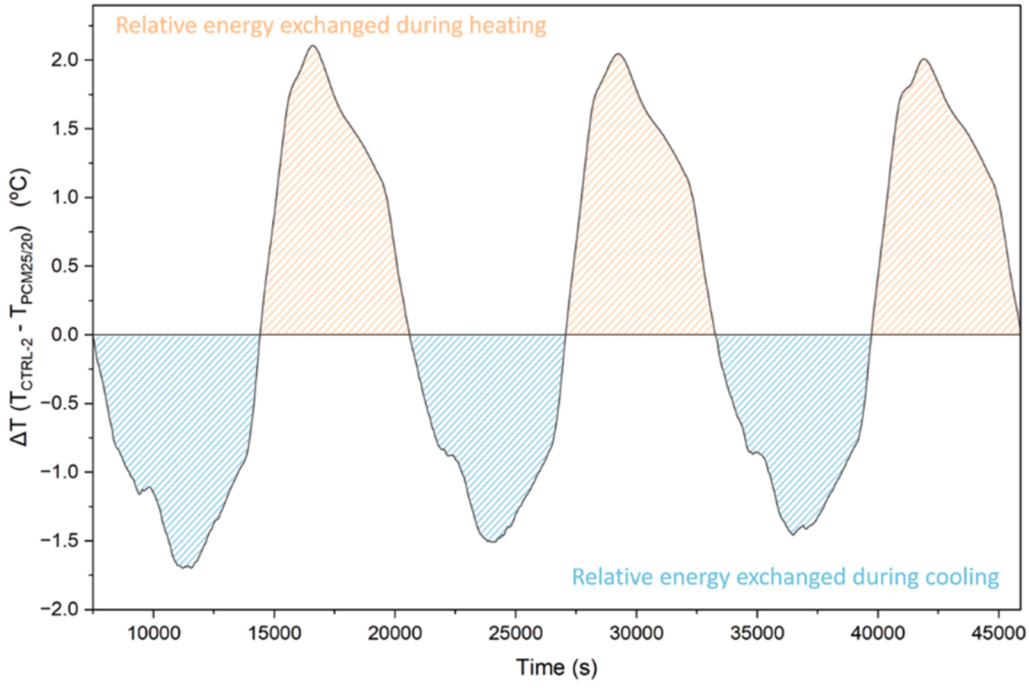

Fig. 17. Time-dependent temperature difference ($\Delta T = T_{CTRL-2}$ - $T_{PCM25/20}$) under hotbox conditions, showing the integrated areas used to estimate the relative energy exchanged in heating and cooling phases.

Table 9
Cycles withstood and final damage scale of durability tests.

Mixtures	Freeze-thaw		Salt attack	
	Cycles withstood	Final damage score (0–10)	Cycles withstood	Final damage score (0–10)
CTRL−1	5	10	14	10
CTRL−2	28	9	28	7
PCM5/0	28	8	28	1
PCM5/20	28	2	28	1
PCM25/0	28	8	28	2
PCM25/20	28	1	28	1

(Fig. 18a). The mixtures incorporating pure lime as binder (PCM5/0 and PCM25/0) reached damage scores of 8, whereas the metakaolin-containing systems demonstrated markedly higher stability. PCM5/20 and PCM25/20 showed only superficial alterations, and PCM25/20 achieved a score of 1, corresponding to an almost intact surface at the end of the test. These trends align with the weight-change curves (Fig. 18b), in which the PCM-bearing mortars exhibit minimal fluctuations throughout the cycling. This behaviour demonstrates that the presence of the silica-supported PCM does not impair frost resistance and, when combined with metakaolin, contributes to a more resilient microstructure capable of accommodating internal stresses associated with ice formation.

A similar pattern emerged under magnesium sulphate crystallisation cycles (Fig. 18 b-c). CTRL−1 again displayed the poorest resistance, failing after 14 cycles with a damage score of 10, while CTRL−2 completed all 28 cycles but experienced progressive decay, reaching a final score of 7 and exhibiting substantial mass loss. All PCM-containing mortars performed significantly better, completing the entire test with only minor deterioration. PCM5/0 and PCM25/0 finished with scores of 1–2, and the mixtures containing metakaolin showed the highest resistance, with both PCM5/20 and PCM25/20 reaching a final score of 1. The corresponding weight-change curves show only tiny variations for the PCM-bearing specimens (Fig. 18d), confirming their limited deterioration throughout the crystallisation cycles.

Taken together, the results from both durability tests demonstrate that incorporating silica-supported form-stable PCMs does not introduce any detrimental effects on the long-term performance of lime mortars. On the contrary, the PCM-containing mortars consistently outperformed the PCM-free references, with the PCM-MK formulations achieving the lowest damage levels under both environmental stressors. These findings are consistent with the microstructural evidence, which shows that the form-stable PCMs integrate seamlessly within the matrix without disrupting its continuity. Overall, the combined contribution of PCM incorporation and the pore-refining action of metakaolin leads to mortars that are simultaneously thermally enhanced and mechanically robust, reinforcing their suitability for lime-based renders exposed to freeze-thaw cycles and salt-rich environments.

Another aspect intrinsically linked to durability and long-term performance is the thermal stability of the PCM itself. While the structural integrity of the composite is one dimension of durability, the PCM's ability to absorb and release heat is equally critical. If this functionality were to degrade over time, the render would remain physically intact yet lose its capacity to regulate temperature, thereby limiting its

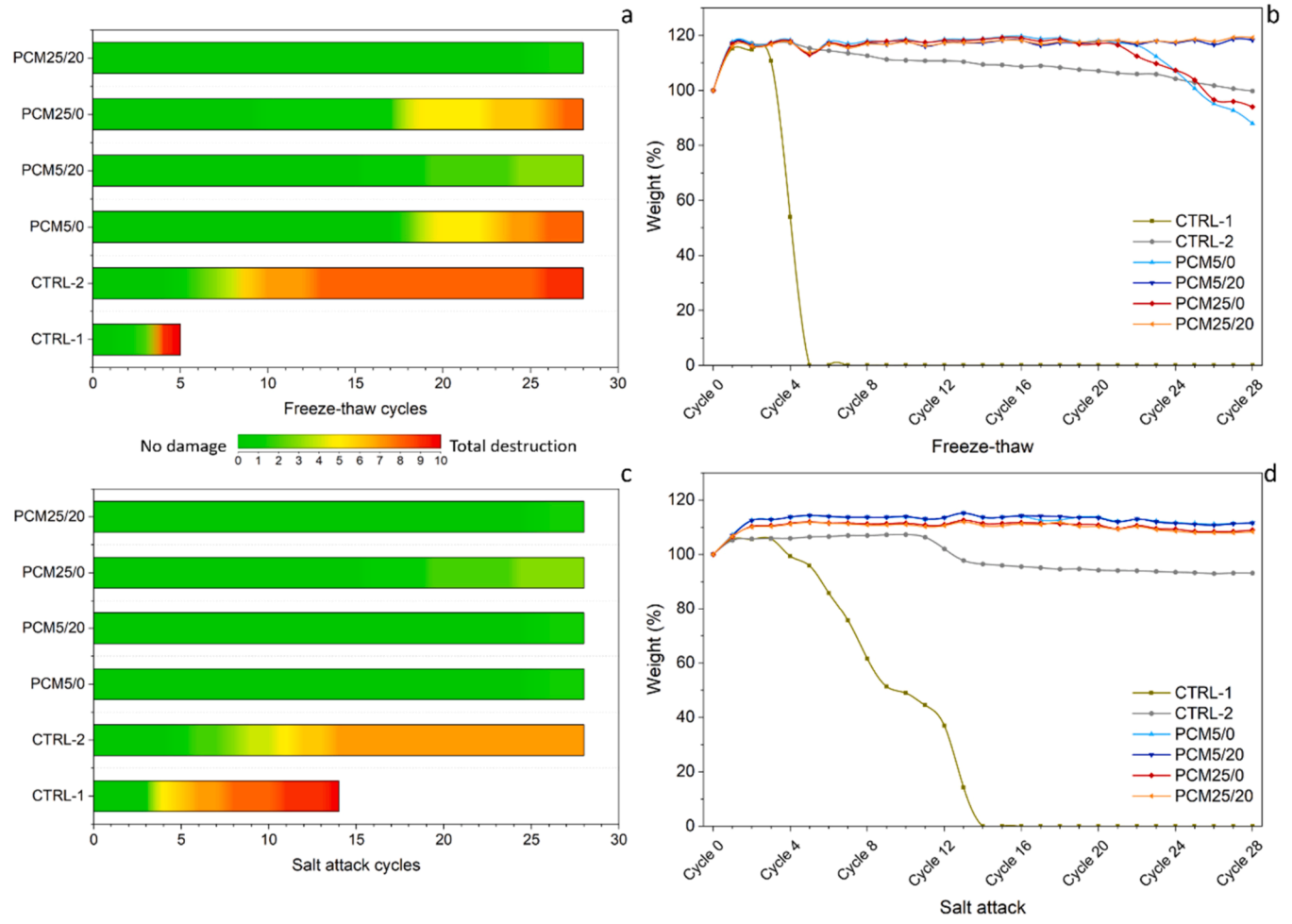

Fig. 18. Durability response of the mortars under freeze-thaw (a-b) and salt attack (c-d); damage progression (a, c) and mass-change evolution during cycling (b, d).

functional lifespan and undermining its role as a truly durable solution. For this reason, the thermal cyclability of the silica-supported PCMs was evaluated, and the corresponding results are presented in Table 10 and Fig. 19.

The data demonstrate outstanding thermal stability across repeated melting-solidification events. Throughout the 40 thermal cycles, both PCMs maintained virtually unchanged phase-change behaviour, with melting and crystallisation enthalpies remaining remarkably consistent. PCM5 exhibited a melting enthalpy of 74.50 ± 0.03 J/g and a crystallisation enthalpy of 76.04 ± 0.50 J/g, while PCM25 reached 93.12 ± 0.03 J/g and 91.61 ± 0.08 J/g for the respective transitions. The extremely low standard deviations associated with these values reflect the high reproducibility of the thermal response and confirm the absence of progressive degradation during cycling. This stability is further evidenced by the DSC thermograms: the melting and crystallisation peaks recorded across the 40 cycles overlap almost perfectly, showing no observable shifts in peak position, peak shape or baseline characteristics (Fig. 19). The absence of peak broadening or attenuation indicates that neither paraffin loss nor alterations to the silica support occurred during repeated phase transitions. Notably, when contextualised against previously reported microencapsulated PCM systems evaluated under the same 40-cycle protocol [16], the present form-stable PCMs demonstrate equally exceptional thermal resilience, thereby further reinforcing the robustness of their cyclability within a consistent comparative framework across distinct PCM technologies. Collectively, these results demonstrate the excellent thermal endurance of the silica-supported PCMs and confirm that their latent heat functionality is fully preserved over extensive cycling, supporting their suitability for long-term integration in lime-based renders.

4. Conclusions

This study provides a comprehensive evaluation of silica-supported, form-stable phase change materials (PCMs) incorporated into lime-based renders, establishing clear links between particle-level interactions, microstructural development, mechanical behaviour, thermal performance and long-term durability. The multi-scale approach adopted demonstrates that these additives can be successfully integrated into air-lime mortars without compromising any of the attributes essential for sustainable construction or heritage conservation. On the contrary, the combined evidence shows that form-stable PCMs can enhance both functional and structural performance when the formulation is carefully optimised.

Compatibility studies revealed that the silica-supported PCMs interact favourably with all components of the mortar system, including lime, metakaolin, the polycarboxylate-based superplasticiser and the starch-derived adhesion promoter. Particle size analysis, optical microscopy and zeta potential measurements consistently showed that neither PCM type induces aggregation, destabilization or other adverse physicochemical interactions in aqueous suspensions.

Building on these findings, the formulation was optimised to ensure suitable workability and rendering performance. Adjusting the dosages of superplasticiser and adhesion promoter enabled all PCM-containing mortars to achieve excellent spreading, cohesion and adhesion, as confirmed by fresh-state testing and visual inspection. These results demonstrate that the challenges commonly reported for PCM-modified mortars in the fresh state can be efficiently mitigated through targeted formulation design.

Table 10
Thermal-cycling stability of the silica-supported PCMs: enthalpies associated with melting and crystallisation and their low variability over 40 cycles.

	ΔH_m (J/g)	ΔH_c (J/g)
PCM5	74.50 ± 0.03	76.04 ± 0.50
PCM25	93.12 ± 0.03	91.61 ± 0.08

Microstructural analysis further confirmed that integrating the silica-supported PCMs does not disrupt the pore network characteristic of lime mortars. Mercury intrusion porosimetry showed that PCM-bearing mixtures largely retain the pore-size distributions of their respective controls, exhibiting only minimal shifts attributable to a subtle filler effect. SEM observations corroborated these findings, revealing continuous matrices free of microcracks, interfacial voids or PCM agglomerates. EDS mapping verified the uniform spatial distribution of the silica carriers within the lime matrix. Together, these results demonstrate that the matrix accommodates the PCMs homogeneously without compromising its microstructural integrity.

The mechanical assessment showed that all PCM-modified mortars developed higher compressive strength than their PCM-free counterparts. The rigid silica carriers acted as mechanically stable inclusions, effectively embedded within the lime matrix, thereby contributing to strength enhancement. The presence of metakaolin provided additional, though modest, improvements, consistent with the limited pozzolanic refinement achievable under the curing conditions employed.

The thermal behaviour characterization confirmed that the silica-supported PCMs retain their latent-heat functionality after incorporation into the lime matrix. Thermal conductivity measurements revealed moderate reductions in λ due to the low conductivity of the PCM-silica composite, while maintaining sufficient heat transfer to ensure efficient activation of the phase-change process. DSC analysis of the pure PCMs demonstrated well-defined and fully reversible phase transitions, providing the latent-heat capacity required for thermal buffering. Complementary leakage tests further confirmed the thermal stability of the form-stable PCMs, showing no paraffin release even under molten conditions at temperatures well above their melting points. Hotbox experiments under dynamic conditions demonstrated the practical implications of this behaviour: all PCM-containing mortars reduced temperature peaks during heating and mitigated temperature drops during cooling, with PCM25 mixtures delivering the strongest and most consistent buffering. Integral analysis of temperature deviations confirmed that both PCMs absorb and release heat throughout the full thermal cycle.

The durability assessment showed that incorporating the silica-supported PCMs does not compromise the weathering resistance. Instead, PCM-bearing mixtures exhibited significantly improved performance under freeze-thaw cycling and magnesium sulfate attack, particularly when combined with metakaolin. These enhancements align with the preserved microstructural integrity observed in MIP and SEM analyses and indicate that the PCMs do not introduce weak zones prone to deterioration. Moreover, the PCMs themselves demonstrated exceptional thermal endurance, maintaining virtually unchanged enthalpies and transition temperatures after 40 cycles, ensuring the long-term preservation of latent heat functionality.

The comprehensive laboratory-scale evidence generated in this work strongly supports the considerable potential of silica-supported PCM-lime mortars as advanced materials for sustainable and energy-efficient building envelopes. Through an extensive multiscale methodology, this study establishes a robust scientific foundation regarding their compatibility, performance, and resilience. Nevertheless, further research focused on large-scale implementation, long-term in-service monitoring, and broader climatic validation would represent a valuable next step to fully consolidate their practical applicability under real operating conditions. In particular, extending the evaluation to real-scale energy performance, prolonged durability scenarios, and long-term cycling behaviour would further strengthen confidence in their widespread adoption, while enabling more precise optimization according to specific construction contexts and environmental demands.

Overall, this study demonstrates that silica-supported, form-stable PCMs can be successfully incorporated into lime-based renders, delivering a dual benefit: enhanced thermal performance through latent heat storage together with the preservation of the mechanical, microstructural and durability properties required for sustainable and heritage-

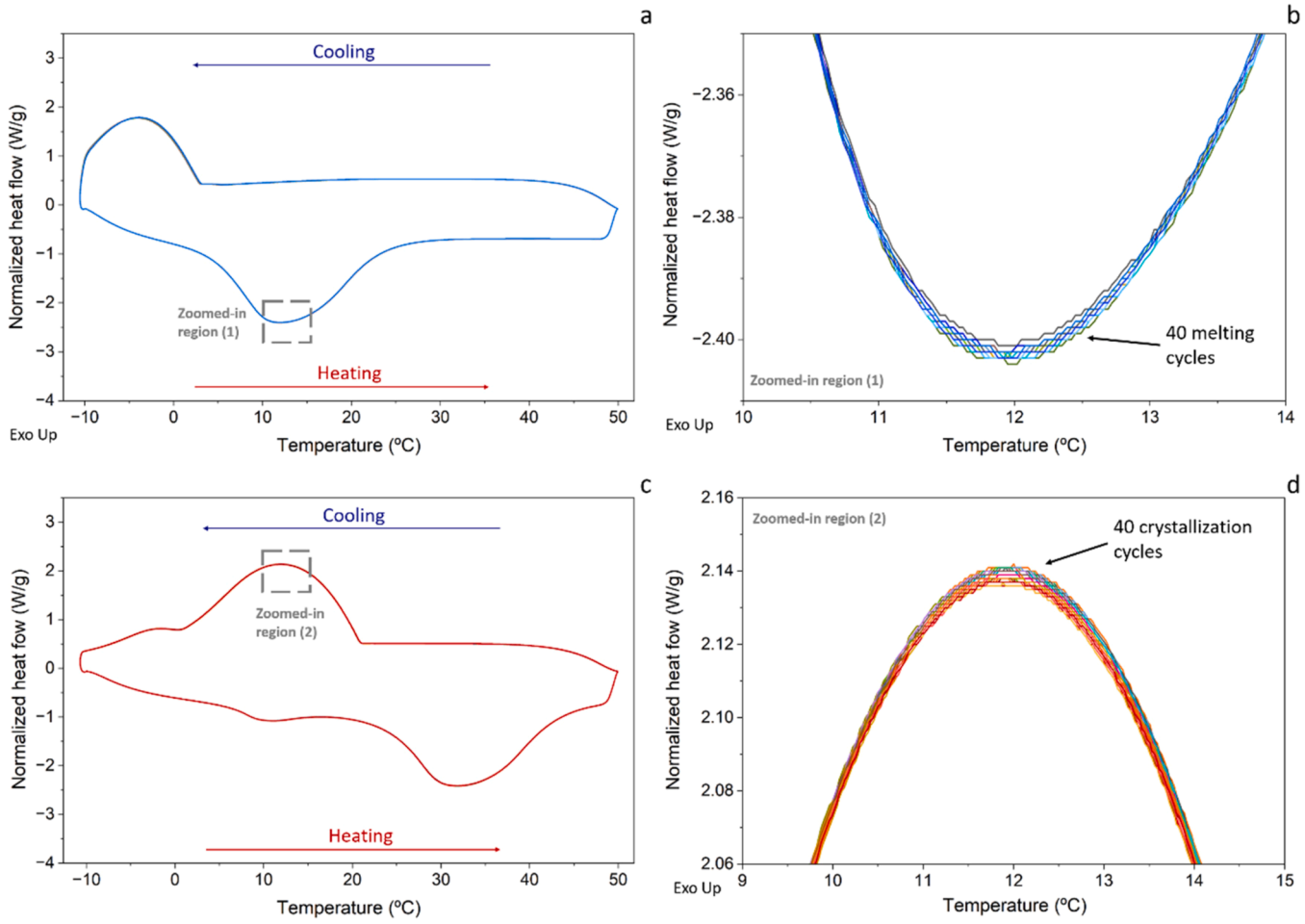

Fig. 19. Thermal-cycling behaviour of the silica-supported PCMs: overlapping DSC curves across 40 cycles demonstrating stable phase-change performance, with (a) full melting-crystallization cycles of PCM5 and the dashed box indicating the region magnified in (b), (b) zoomed view of the melting region of PCM5, (c) full cycles of PCM25 with the dashed box marking the area enlarged in (d), and (d) zoomed view of the crystallization region of PCM25.

compatible materials. The excellent thermal stability of the PCMs, the absence of detrimental microstructural effects, the improved durability and the measurable thermal moderation collectively highlight their potential for energy-efficient building envelopes. These findings provide a robust scientific basis for the implementation of form-stable PCM-lime mortars in both restoration and modern construction, and emphasise the importance of formulation optimization to ensure long-term functional and structural performance.

CRediT authorship contribution statement

Íñigo Navarro-Blasco: Supervision, Resources, Project administration, Methodology, Funding acquisition, Data curation, Conceptualization. **Alvarez José Ignacio:** Writing – review & editing, Visualization, Supervision, Resources, Project administration, Funding acquisition, Conceptualization. **Loucas Kyriakou:** Writing – review & editing, Conceptualization. **José María Fernández:** Writing – review & editing, Conceptualization. **Andrea Rubio-Aguinaga:** Writing – original draft, Visualization, Validation, Methodology, Investigation, Formal analysis, Data curation, Conceptualization.

Declaration of Generative AI and AI-assisted technologies in the writing process

During the preparation of this work the authors used ChatGPT (Open AI) for language improvement purposes only. After using this service, the authors reviewed and edited the content as needed and take full responsibility for the content of the published article.

Declaration of Competing Interest

The authors declare that they have no known competing financial interests or personal relationships that could have appeared to influence the work reported in this paper.

Acknowledgements

The authors express their gratitude for the technical support provided by Cristina Luzuriaga. We also appreciate the material supplied by Calinsa S.A. Navarra and CTH Navarra.

This work was co-funded by the European Union's Horizon Europe research and innovation programme, under Grant Agreement No 101123293 (SINCERE- The Second Life of Modern Period Architecture: Resilient and Adaptive Renovation towards Net-Zero Carbon Heritage Buildings) and by Gobierno de España, Ministerio de Ciencia e Innovación (MICINN/AEI/10.13039/501100011033), grant PID2020–119975RB-I00, LIMORTHER. Andrea Rubio-Aguinaga has been granted a fellowship of the programme of the Gobierno de España, Ministerio de Universidades FPU21/04961.

Appendix A. Supporting information

Supplementary data associated with this article can be found in the online version at doi:10.1016/j.conbuildmat.2026.147166.

Data availability

Data will be made available on request.

References

[1] European Commission, A Renovation Wave for Europe – Greening our buildings, creating jobs, improving lives, Brussels, 2020.
[2] Buildings Performance Institute Europe (BPIE), Europe's Buildings Under the Microscope: A country-by-country review of the energy performance of buildings, Brussels, 2011.
[3] European Commission, The European Green Deal, Brussels, 2019.
[4] European Commission, Nearly-zero energy and zero-emission buildings. Energy Performance of Buildings Directive (EPBD) recast – directive (EU) 2024/1275, 2025.
[5] IEA, Net Zero by 2050 - A Roadmap for the Global Energy Sector, Paris, 2021.
[6] M. Deshmukh, M. Yadav, Optimizing thermal efficiency of building envelopes with sustainable composite materials, Buildings 15 (2025), https://doi.org/10.3390/buildings15020230.
[7] K. Ghazwani, T. Beach, Y. Rezgui, Energy retrofitting using advanced building envelope materials for sustainable housing: A review, Build. Environ. 267 (2025), https://doi.org/10.1016/j.buildenv.2024.112243.
[8] F. Ascione, N. Bianco, R.F. De Masi, G.M. Mauro, G.P. Vanoli, Design of the Building Envelope: A Novel Multi-Objective Approach for the Optimization of Energy Performance and Thermal Comfort, Sustainability 7 (2015) 10809–10836, https://doi.org/10.3390/su70810809.
[9] J. Narbuts, R. Vanaga, Revolutionizing the Building Envelope: A Comprehensive Scientific Review of Innovative Technologies for Reduced Emissions, Environ. Clim. Technol. 27 (2023) 724–737, https://doi.org/10.2478/rtuect-2023-0053.
[10] L.F. Cabeza. Advances in thermal energy storage systems: methods and applications, 1st ed., Woodhead Publishing, Cambridge, England, 2015.
[11] R.G. Elenga, L. Zhu, S. Defilla, Performance evaluation of different building envelopes integrated with phase change materials in tropical climates, Energy Built Environ. 6 (2025) 332–346, https://doi.org/10.1016/j.enbenv.2023.11.008.
[12] L.Y. Zhang, Q.Z. Zhang, L.W. Jin, X. Cui, X.H. Yang, Energy, economic and environmental (3E) analysis of residential building walls enhanced with phase change materials, J. Build. Eng. 84 (2024), https://doi.org/10.1016/j.jobe.2024.108503.
[13] A. Rubio-Aguinaga, L. Kyriakou, J.M. Fernández, I. Navarro-Blasco, S. Pavia, J. I. Álvarez, Sustainability of PCM-lime mortars for heritage retrofitting: Carbon footprint and impact on energy demand across climates, Case Stud. Constr. Mater. 23 (2025) e05294, https://doi.org/10.1016/j.cscm.2025.e05294.
[14] M. Theodoridou, L. Kyriakou, I. Ioannou, PCM-enhanced Lime Plasters for Vernacular and Contemporary Architecture, Energy Procedia 97 (2016) 539–545, https://doi.org/10.1016/j.egypro.2016.10.070.
[15] V.V. Rao, R. Parameshwaran, V.V. Ram, PCM-mortar based construction materials for energy efficient buildings: A review on research trends, Energy Build. 158 (2018) 95–122, https://doi.org/10.1016/j.enbuild.2017.09.098.
[16] A. Rubio-Aguinaga, L. Kyriakou, J.M. Fernández, Í. Navarro-Blasco, J.I. Álvarez, Microstructural analysis of bio-based PCM-enhanced lime mortars: Durability and energy efficiency for sustainable buildings, Constr. Build. Mater. 481 (2025) 141569, https://doi.org/10.1016/j.conbuildmat.2025.141569.
[17] L. Haurie, S. Serrano, M. Bosch, A.I. Fernandez, L.F. Cabeza, Single layer mortars with microencapsulated PCM: Study of physical and thermal properties, and fire behaviour, Energy Build. 111 (2016) 393–400, https://doi.org/10.1016/j.enbuild.2015.11.028.
[18] M. Salihi, M.El Fiti, Y. Harmen, Y. Chhiti, A. Chebak, F.E.M. Alaoui, M. Achak, F. Bentiss, C. Jama, Evaluation of global energy performance of building walls integrating PCM: Numerical study in semi-arid climate in Morocco, Case Stud. Constr. Mater. 16 (2022), https://doi.org/10.1016/j.escm.2022.e00979.
[19] A. Rubio-Aguinaga, J.M. Fernandez, I. Navarro-Blasco, J.I. Alvarez, Study on the Interaction of Polymeric Chemical Additives with Phase Change Materials in Air Lime Renders, Polymers 16 (2024) 1121, https://doi.org/10.3390/polym16081121.
[20] S. Sharwan, P. Sikarwar, B. Mazumdar, Recent innovations in support materials for shape-stable organic composite phase change materials: A comprehensive review, Sol. Energy Mater. Sol. CELLS 272 (2024), https://doi.org/10.1016/j.solmat.2024.112910.
[21] K.Y. Weng, X.Y. Xu, Y.Y. Chen, X.L. Li, C.Y. Qing, D.Q. Zou, Development and applications of multifunctional microencapsulated PCMs: A comprehensive review, Nano Energy 122 (2024), https://doi.org/10.1016/j.nanoen.2024.109308.
[22] M. Frigione, M. Lettieri, A. Sarcinella, J.B. de Aguiar, Sustainable polymer-based Phase Change Materials for energy efficiency in buildings and their application in aerial lime mortars, Constr. Build. Mater. 231 (2020) 117149, https://doi.org/10.1016/j.conbuildmat.2019.117149.
[23] P.K.S. Rathore, S.K. Shukla, Potential of macroencapsulated PCM for thermal energy storage in buildings: A comprehensive review, Constr. Build. Mater. 225 (2019) 723–744, https://doi.org/10.1016/j.conbuildmat.2019.07.221.
[24] A. Rubio-Aguinaga, J.M. Fernández, Í. Navarro-Blasco, J.I. Álvarez, Air lime renders with microencapsulated phase change materials: Assessment of microstructural and thermal properties, Constr. Build. Mater. 452 (2024) 138862, https://doi.org/10.1016/j.conbuildmat.2024.138862.
[25] A. Rubio-Aguinaga, L. Kyriakou, J. María Fernández, Í. Navarro-Blasco, J. I. Álvarez, Silica-Supported Form-Stable Phase Change Materials for Enhancing Thermal Performance in Lime Mortars. 4th International Conference of Sustainable Building Materials, Eindhoven, 2025.
[26] M. Gandhi, A. Kumar, R. Elangovan, C.S. Meena, K.S. Kulkarni, A. Kumar, G. Bhanot, N.R. Kapoor, A Review on Shape-Stabilized Phase Change Materials for Latent Energy Storage in Buildings, Sustainability 12 (2020), https://doi.org/10.3390/su12229481.
[27] D. Das, R. Crosby, M.C. Paul, A comprehensive review on the form stable phase change materials for storing renewable heat preparation, characterization and application, J. Energy Storage 110 (2025) 115284, https://doi.org/10.1016/j.est.2024.115284.
[28] W.X. Wu, W. Wu, S.F. Wang, Form-stable and thermally induced flexible composite phase change material for thermal energy storage and thermal management applications, Appl. Energy 236 (2019) 10–21, https://doi.org/10.1016/j.apenergy.2018.11.071.
[29] T.W. Fu, W.Z. Wang, G.Y. Fang, Thermal properties and applications of form-stable phase change materials for thermal energy storage and thermal management: A review, Energy STORAGE 6 (2024), https://doi.org/10.1002/est2.533.
[30] X.B. Huang, X. Chen, A. Li, D. Atinafu, H.Y. Gao, W.J. Dong, G. Wang, Shape-stabilized phase change materials based on porous supports for thermal energy storage applications, Chem. Eng. J. 356 (2019) 641–661, https://doi.org/10.1016/j.cej.2018.09.013.
[31] X.S. Du, J.H. Qiu, S. Deng, Z.L. Du, X. Cheng, H.B. Wang, Alkylated Nanofibrillated Cellulose/Carbon Nanotubes Aerogels Supported Form-Stable Phase Change Composites with Improved n-Alkanes Loading Capacity and Thermal Conductivity, ACS Appl. Mater. Interfaces 12 (2020) 5695–5703, https://doi.org/10.1021/acsami.9b17771.
[32] H.Z. Hong, Y. Pan, H.X. Sun, Z.Q. Zhu, C.H. Ma, B. Wang, W.D. Liang, B.P. Yang, A. Li, Superwetting polypropylene aerogel supported form-stable phase change materials with extremely high organics loading and enhanced thermal conductivity, Sol. Energy Mater. Sol. Cells 174 (2018) 307–313, https://doi.org/10.1016/j.solmat.2017.09.026.
[33] M.D. Veiga, A. Fragata, A.L. Velosa, A.C. Magalhaes, G. Margalha, Lime-Based Mortars: Viability for Use as Substitution Renders in Historical Buildings, Int J. Architectural Herit. 4 (2010) 177–195, https://doi.org/10.1080/15583050902914678.
[34] A. Manoharan, C. Umarani, Lime Mortar, a boon to the environment: characterization case study and overview, Sustainability 14 (2022), https://doi.org/10.3390/su14116481.
[35] F.Pietro Campo, M. Grosso, Lime Based Construction Materials as a Carbon Sink, Key Eng. Mater. 922 (2022) 139–145, https://doi.org/10.4028/p-t8k30r.
[36] J. Ryan, M. Bussmann, N. DeMartini, CFD Modelling of Calcination in a Rotary Lime Kiln, PROCESSES 10 (2022), https://doi.org/10.3390/pr10081516.
[37] J.T. Ju, H.B. Cao, W.K. Guo, N. Luo, Q.M. Zhang, Y.G. Wang, Experimental Study on Calcination of Portland Cement Clinker Using Different Contents of Stainless Steel Slag, MATERIALS 17 (2024), https://doi.org/10.3390/ma17102305.
[38] Z. Pavlík, A. Trník, M. Keppert, M. Pavlíková, J. Zumár, R. Cerny, Experimental Investigation of the Properties of Lime-Based Plaster-Containing PCM for Enhancing the Heat-Storage Capacity of Building Envelopes, Int. J. Thermophys. 35 (2014) 767–782, https://doi.org/10.1007/s10765-013-1550-8.
[39] V.Z. Vargas, L.J. Claros-Marfil, G.F.B. Sandoval, B.H. Rojas, A.G. Santos, FcoJ. N. González, Experimental assessment of energy storage in microencapsulated paraffin PCM Cement mortars, Case Stud. Constr. Mater. 20 (2024) e02959, https://doi.org/10.1016/j.cscm.2024.e02959.
[40] N.B. Srinivasaraonaik, L.P. Singh, S. Sinha, I. Tyagi, G. Mittal, Studies on thermal properties of microencapsulated eutectic phase change material incorporated different mortar mixes, Int. J. Energy Res. 45 (2021) 2488–2497, https://doi.org/10.1002/er.5943.
[41] R. Illampas, I. Rigopoulos, I. Ioannou, Influence of microencapsulated Phase Change Materials (PCMs) on the properties of polymer modified cementitious repair mortar, J. Build. Eng. 40 (2021), https://doi.org/10.1016/j.jobe.2021.102328.
[42] S.S. Lucas, J.L. Barroso de Aguiar, Evaluation of latent heat storage in mortars containing microencapsulated paraffin waxes – a selection of optimal composition and binders, Heat. Mass. Transf. /Waerme- Und Stoff. (2019), https://doi.org/10.1007/s00231-019-02594-1.
[43] E. Erkizia, C. Strunz, J.L. Dauvergne, G. Goracci, I. Peralta, A. Serrano, A. Ortega, B. Alonso, F. Zanoni, M. Duengfelder, J.S. Dolado, J.J. Gaitero, C. Mankel, E. Koenders, Study of paraffinic and biobased microencapsulated PCMs with reduced graphene oxide as thermal energy storage elements in cement-based

materials for building applications, J. Energy Storage 84 (2024), https://doi.org/10.1016/j.est.2024.110675.
[44] K. Stejskalová, D. Bujdos, L. Procházka, B. Smetana, S. Zlá, J. Teslík, Mechanical, thermal, and fire properties of composite materials based on gypsum and PCM, Materials 15 (2022), https://doi.org/10.3390/ma15031253.
[45] V.D. Cao, S. Pilehvar, C. Salas-Bringas, A.M. Szczotok, J.F. Rodriguez, M. Carmona, N. Al-Manasir, A.L. Kjoniksen, Microencapsulated phase change materials for enhancing the thermal performance of Portland cement concrete and geopolymer concrete for passive building applications, Energy Convers. Manag. 133 (2017) 56–66, https://doi.org/10.1016/j.enconman.2016.11.061.
[46] A. Sarcinella, J.L.B. de Aguiar, C. Jesus, M. Frigione, Thermal properties of PEG-based form-stable Phase Change Materials (PCMs) incorporated in mortars for energy efficiency of buildings, J. Energy Storage 67 (2023), https://doi.org/10.1016/j.est.2023.107545.
[47] S. Cunha, A. Sarcinella, N. Reis, J. Aguiar, M. Frigione, High temperature performance of cement mortars with incorporation of PEG-based form-stable Phase Change Materials, Constr. Build. Mater. 438 (2024) 136946, https://doi.org/10.1016/j.conbuildmat.2024.136946.
[48] D. Zhou, S. Xiao, Y. Liu, Preparation and characterization of innovative cement mortar incorporating fatty acid/expanded graphite composite phase change material for thermal energy storage, Sci. Rep. 14 (2024) 16523, https://doi.org/10.1038/s41598-024-67573-x.
[49] D. Kumar, M. Alam, J. Sanjayan, M. Haris, Comparative analysis of form-stable phase change material integrated concrete panels for building envelopes, Case Stud. Constr. Mater. 18 (2023) e01737, https://doi.org/10.1016/j.cscm.2022.e01737.
[50] A. Sarcinella, Physical properties of an eco-sustainable, form-stable phase change material included in aerial-lime-based mortar intended for different climates, Materials 15 (2022) 1192.
[51] A. Garzulino, Energy Efficiency: A Multi-Criteria Evaluation Method for the Intervention on Built Heritage, Sustainability 12 (2020), https://doi.org/10.3390/su12219223.
[52] European Committee for Standarization, UNE-EN 1015-3 Methods of Test for Mortar for Masonry. Part 3: Determination of consistence of fresh mortar (by flow table), EN, (2006).
[53] European Committee for Standarization, UNE-EN 1015-6 Methods of test for mortar for masonry - Part 6: Determination of bulk density of fresh mortar, (1999).
[54] European Committee for Standardization, UNE-EN 1015-7:1999 Methods of Test for Mortar for Masonry. Part 7: Determination of Air Content of Fresh Mortar, EN, (1999).
[55] AENOR, UNE- 83-816-93 Test methods. Fresh Mortars. Determination of water retentivity, (1993).
[56] M.N. Sam, A. Caggiano, C. Mankel, E. Koenders, A Comparative Study on the Thermal Energy Storage Performance of Bio-Based and Paraffin-Based PCMs Using DSC Procedures, MATERIALS 13 (2020), https://doi.org/10.3390/ma13071705.
[57] P. Gabbott. Principles of Thermal Analysis and Calorimetry, 2008, 10.1039/9781847551764-00010.
[58] T. Hatakeyama, F.X. Quinn. Thermal analysis: Fundamentals and Applications to Polymer Science, 2nd ed., John Wiley & Sons, New York, 1995.
[59] T.H. Bui, G.T. Nguyen, Enhanced Thermal Energy Storage of n-Octadecane-Impregnated Mesoporous Silica as a Novel Shape-Stabilized Phase Change Material, ACS Omega 7 (2022) 12222–12230, https://doi.org/10.1021/acsomega.2c00623.
[60] Y. Li, M.Y. Dong, W. Song, X.Y. Liang, Y.W. Chen, Y.F. Liu, Preparation and Characterization of Paraffin/Mesoporous Silica Shape-Stabilized Phase Change Materials for Building Thermal Insulation, MATERIALS 14 (2021), https://doi.org/10.3390/ma14071775.
[61] R. Shadnia, L.Y. Zhang, P.W. Li, Experimental study of geopolymer mortar with incorporated PCM, Constr. Build. Mater. 84 (2015) 95–102, https://doi.org/10.1016/j.conbuildmat.2015.03.066.
[62] B.A. Young, G. Falzone, Z.H. Wei, G. Sant, L. Pilon, Reduced-scale experiments to evaluate performance of composite building envelopes containing phase change materials, Constr. Build. Mater. 162 (2018) 584–595, https://doi.org/10.1016/j.conbuildmat.2017.11.160.
[63] European Committee for Standardization (CEN), EN 1367-1:2007 - Tests for thermal and weathering properties of aggregates - Part 1: Determination of resistance to freezing and thawing, 2008.
[64] European Committee for Standardization (CEN), EN 1367-2:2009 - Tests for thermal and weathering properties of aggregates - Part 2: Magnesium sulfate test, 2009.
[65] A. Rubio-aguinaga, J.M. Fernández, Í. Navarro-blasco, J.I. Álvarez, Green way of improving the thermal efficiency of mortars by the addition of biobased phase change materials, in: SUBLime Conference 2024 - Towards the Next Generation of Sustainable Masonry Systems: Mortars, Renders, Plasters and Other Challenges, MATEC Web of Conferences, Funchal, Portugal, 2024. https://doi.org/10.1051/matecconf/202440303007.
[66] ASTM International, Standard Test Method for Density of Hydraulic Cement (C188 − 17), (2023). https://doi.org/10.1520/C0188-17R23.
[67] M. Thommes, K. Kaneko, A.V. Neimark, J.P. Olivier, F. Rodriguez-Reinoso, J. Rouquerol, K.S.W. Sing, Physisorption of gases, with special reference to the evaluation of surface area and pore size distribution (IUPAC Technical Report), Pure Appl. Chem. 87 (2015) 1051–1069, https://doi.org/10.1515/pac-2014-1117.
[68] S. Lowell, Joan E. Shields, Martin A. Thomas, Matthias Thommes, Characterization of Porous Solids and Powders Surface Area. Pore Size and Density, 1st ed., Springer, Dordrecht, 2004 https://doi.org/10.1007/978-1-4020-2303-3.
[69] Y.J. Chen, J.H. Liu, X.H. Li, Z.J. Zhang, Z.W. Li, Mesoporous silica-loaded phosphorus-modified hexadecanol nanocomposites for flame-retardant and shape-stabilized phase change materials, Compos. Part A-Appl. Sci. Manuf. 199 (2025), https://doi.org/10.1016/j.compositesa.2025.109227.
[70] D. Chen, Y. Chen, X.W. Guo, W.W. Tao, J.B. Wang, S.F. Gao, J.K. Gao, Mesoporous silica nanoparticles with wrinkled structure as the matrix of myristic acid for the preparation of a promising new shape-stabilized phase change material via simple method, RSC Adv. 8 (2018) 34224–34231, https://doi.org/10.1039/c8ra06536e.
[71] A. Ishihara, T. Hashimoto, H. Nasu, Large Mesopore Generation in an Amorphous Silica-Alumina by Controlling the Pore Size with the Gel Skeletal Reinforcement and Its Application to Catalytic Cracking, Catalysts 2 (2012) 368–385, https://doi.org/10.3390/catal2030368.
[72] G. Dragan, V. Kutarov, E. Schieferstein, A. Iorgov, Adsorption Hysteresis in Open Slit-like Micropores, Molecules 26 (2021), https://doi.org/10.3390/molecules26165074.
[73] C. Bläker, J. Muthmann, C. Pasel, D. Bathen, Characterization of Activated Carbon Adsorbents - State of the Art and Novel Approaches, Chembioeng Rev. 6 (2019) 119–138, https://doi.org/10.1002/cben.201900008.
[74] T.T. Qian, J.H. Li, Y. Deng, Pore structure modified diatomite-supported PEG composites for thermal energy storage, Sci. Rep. 6 (2016), https://doi.org/10.1038/srep32392.
[75] J.M. Morales, A. Moragues, J. El Haskouri, C. Guillem, J. Latorre, S. Murcia-Mascarós, A. Beltrán, D. Beltrán, P. Amorós, Low-Cost Synthesis of Bimodal Mesoporous Silica-Based Materials by Pseudomorphic Transformation, Chempluschem 80 (2015) 1014–1028, https://doi.org/10.1002/cplu.201402383.
[76] A. Arizzi, G. Cultrone, Aerial lime-based mortars blended with a pozzolanic additive and different admixtures: A mineralogical, textural and physical-mechanical study, Constr. Build. Mater. 31 (2012) 135–143, https://doi.org/10.1016/j.conbuildmat.2011.12.069.
[77] A. Duran, J.F. Gonzalez-Sanchez, J.M. Fernandez, R. Sirera, I. Navarro-Blasco, J. I. Alvarez, Influence of Two Polymer-Based Superplasticizers (Poly-naphthalene Sulfonate, PNS, and Lignosulfonate, LS) on Compressive and Flexural Strength, Freeze-Thaw, and Sulphate Attack Resistance of Lime-Metakaolin Grouts, Polymers 10 (2018) 824, https://doi.org/10.3390/polym10080824.
[78] D. Xu, G.D. Qi, D.M. Wang, D.J. Zhang, S. Zhang, Competitive mechanisms of hydration and carbonation in hydraulic lime under natural and accelerated carbonation (3% CO2), J. Build. Eng. 111 (2025), https://doi.org/10.1016/j.jobe.2025.113357.
[79] M. Frigione, A. Sarcinella, J.L.B. de Aguiar, Development and Performance of Eco-Sustainable Form-Stable Phase Change Materials (PCMs) for Mortars to Be Applied in Buildings Located in Different Climatic Areas, COATINGS 13 (2023), https://doi.org/10.3390/coatings13020258.
[80] V. Zetola, L.J. Claros-Marfil, A.G. Santos, F.J.N. González, Effect of Paraffin and Silica Matrix Phase Change Materials on Properties of Portland Cement Mortars, MATERIALS 14 (2021), https://doi.org/10.3390/ma14040921.
[81] M.R. Islam, X. Li, Application of from-stable paraffin/nano-silica phase change materials for thermal energy storage in mortar, Int. Adv. Res. J. Sci. Eng. Technol. (2023), https://doi.org/10.17148/IARJSET.2023.10502.
[82] A. Sarcinella, J.L.B. de Aguiar, M. Frigione, Physical Properties of Eco-Sustainable Form-Stable Phase Change Materials Included in Mortars Suitable for Buildings Located in Different Continental Regions, MATERIALS 15 (2022), https://doi.org/10.3390/ma15072497.
[83] H. Abbasi Hattan, M. Madhkhan, A. Marani, Thermal and mechanical properties of building external walls plastered with cement mortar incorporating shape-stabilized phase change materials (SSPCMs), Constr. Build. Mater. 270 (2021) 121385, https://doi.org/10.1016/j.conbuildmat.2020.121385.
[84] A.S. Silva, A. Gameiro, J. Grilo, R. Veiga, A. Velosa, Long-term behavior of lime-metakaolin pastes at ambient temperature and humid curing condition, Appl. Clay Sci. 88–89 (2014) 49–55, https://doi.org/10.1016/j.clay.2013.12.016.
[85] Y. Yan, S.C. King, M. Li, T. Galy, M. Marszewski, J.S. Kang, L. Pilon, Y.J. Hu, S. H. Tolbert, Exploring the Effect of Porous Structure on Thermal Conductivity in Templated Mesoporous Silica Films, J. Phys. Chem. C. 123 (2019) 21721–21730, https://doi.org/10.1021/acs.jpcc.9b03767.
[86] L. An, M. Di Luigi, D. Petit, Y. Hu, Y.J. Chen, J.N. Armstrong, Y.G.C. Li, S.Q. Ren, Nanoengineering Porous Silica for Thermal Management, ACS Appl. Nano Mater. 5 (2022), https://doi.org/10.1021/acsanm.1c04354.
[87] P. Bose, V.A. Amirtham, A review on thermal conductivity enhancement of paraffinwax as latent heat energy storage material, Renew. & Sustain. ENERGY Rev. 65 (2016) 81–100, https://doi.org/10.1016/j.rser.2016.06.071.
[88] R.A. Mitran, S. Ionita, D. Lincu, D. Berger, C. Matei, A Review of Composite Phase Change Materials Based on Porous Silica Nanomaterials for Latent Heat Storage Applications, Molecules 26 (2021), https://doi.org/10.3390/molecules26010241.
[89] G.L. Chen, F.L. Li, P.F. Jing, J.Y. Geng, Z.K. Si, Effect of Pore Structure on Thermal Conductivity and Mechanical Properties of Autoclaved Aerated Concrete, Materials 14 (2021), https://doi.org/10.3390/ma14020339.
[90] S. Kahwaji, M.A. White, Organic Phase Change Materials for Thermal Energy Storage: Influence of Molecular Structure on Properties, Molecules 26 (2021), https://doi.org/10.3390/molecules26216635.
[91] M. Zare, K.S. Mikkonen, Phase change materials for life science applications, Adv. Funct. Mater. 33 (2023), https://doi.org/10.1002/adfm.202213455.
[92] A. Said, A. Salah, G.A. Fattah, Enhanced Thermo-Optical Switching of Paraffin-Wax Composite Spots under Laser Heating, Materials 10 (2017), https://doi.org/10.3390/ma10050525.
[93] W. Mhike, W.W. Focke, J.P. Mofokeng, A.S. Luyt, Thermally conductive phase-change materials for energy storage based on low-density polyethylene, soft

Fischer–Tropsch wax and graphite, Thermochim. Acta 527 (2012) 75–82, https://doi.org/10.1016/j.tca.2011.10.008.
[94] Z.H. Rao, G.Q. Zhang, Thermal properties of paraffin wax-based composites containing graphite, Energy Sources Part. A Recovery Util. Environ. Eff. 33 (2011) 587–593, https://doi.org/10.1080/15567030903117679.
[95] L. Navarro, A. Solé, M. Martín, C. Barreneche, L. Olivieri, J.A. Tenorio, L.F. Cabeza, Benchmarking of useful phase change materials for a building application, Energy Build. 182 (2019) 45–50, https://doi.org/10.1016/j.enbuild.2018.10.005.
[96] J. Giro-Paloma, R. Al-Shannaq, A.I. Fernández, M.M. Farid, Preparation and characterization of microencapsulated phase change materials for use in building applications, Materials 9 (2016), https://doi.org/10.3390/ma9010011.